METRIC

TDL-0634
REVISION BASIC

# CHARACTERIZATION TEST REPORT FOR THE MNEMONICS-UCF WIRELESS SURFACE ACOUSTIC WAVE SENSOR SYSTEM

# TRANSDUCER DEVELOPMENT LABORATORY

# FEBRUARY 28, 2013

# ENGINEERING AND TECHNOLOGY DIRECTORATE

National Aeronautics and
Space Administration

**John F. Kennedy Space Center**

KSC FORM 4-501 (REV. 4/94)

# CHARACTERIZATION TEST REPORT FOR THE MNEMONICS-UCF WIRELESS SURFACE ACOUSTIC WAVE SENSOR SYSTEM

# TRANSDUCER DEVELOPMENT LABORATORY

Prepared by:

_____

Joshua J. Duncan, ESC-28
ESC Engineer

Concurrence:

_____

Robert C. Smith, Jr., ESC-28
ESC Engineer

Approved by:

_____

N. N. "Mike" Blalock, ESC-48
ESC Transducer Lab Lead

This Revision Supersedes All Previous Editions of This Document

## FEBRUARY 28, 2013

## JOHN F. KENNEDY SPACE CENTER, NASA

| RECORD OF REVISIONS | | |
|---|---|---|
| **REV LTR** | **DESCRIPTION** | **DATE** |
| | Interim Report 1 | December 16, 2011 |
| | Basic Issue | February 28, 2013 |

# CONTENTS

# FIGURES

## TABLES

## ABBREVIATIONS, ACRONYMS, AND SYMBOLS

| Term | Definition |
|------|------------|
| A | ampere |
| ABS | acrylonitrile butadiene styrene |
| AC | alternating current |
| ADC | analog-to-digital converter |
| ASR&D | Applied Sensor Research & Development Corporation |
| AVO | Avoid Verbal Orders |
| °C | degrees Celsius |
| dB | decibel |
| dBμV | decibels referenced to one microvolt |
| DIP | dual in-line package |
| DC | direct current |
| ECN | equipment control number |
| EDL | Engineering Development Laboratory |
| EMC | electromagnetic compatibility |
| EMI | electromagnetic interference |
| EML | Electromagnetic Effects Laboratory |
| ESC | Engineering Services Contract |
| FCC | Federal Communications Commission |
| FFT | Fast Fourier Transform |
| FS | full scale |
| GB | gigabytes |
| GCF | gas correction factor |
| GHz | gigahertz |
| GPIB | General Purpose Interface Bus |
| GS/s | gigasamples per second |
| GSM | Global System for Mobile Communications |
| GUI | graphical user interface |
| H2 or $H_2$ | hydrogen |

| | |
|---|---|
| HDPE | high-density polyethylene |
| HP-IB | Hewlett-Packard Interface Bus |
| hr | hour |
| HVAC | heating, ventilating, and air conditioning |
| Hz | hertz |
| IC | integrated circuit |
| IEEE | Institute of Electrical and Electronics Engineers |
| ISM | industrial, scientific and medical |
| kHz | kilohertz |
| KSC | John F. Kennedy Space Center |
| LED | light-emitting diode |
| LN2 | liquid nitrogen |
| m | meter |
| MEK | methyl ethyl ketone |
| MHz | megahertz |
| min | minute |
| MNI | Mnemonics, Inc. |
| MSL | Materials Science Laboratory |
| MSFC | George C. Marshall Space Flight Center |
| NASA | National Aeronautics and Space Administration |
| ns | nanosecond |
| PCMCIA | Personal Computer Memory Card International Association |
| ppm | parts per million |
| PSD | power spectral density |
| PVC | polyvinyl chloride |
| RAM | random-access memory |
| RBW | resolution bandwidth |
| RF | radio frequency |
| RFA | Radio Frequency Authorization |
| S/N | serial number |
| SAW | surface acoustic wave |

| | |
|---|---|
| SBIR | Small Business Innovation Research |
| SCCM | standard cubic centimeters per minute |
| SLPM | standard liters per minute |
| STTR | Small Business Technology Transfer |
| TC | technical contact |
| TDL | Transducer Development Laboratory |
| UCF | University of Central Florida |
| V | volt |
| VBW | video bandwidth |
| WAC | Work Authorization Control |
| $\sigma$ | standard deviation |
| " | inch |

**CHARACTERIZATION TEST REPORT FOR THE MNEMONICS-UCF WIRELESS SURFACE ACOUSTIC WAVE SENSOR SYSTEM**

## 1. INTRODUCTION

### 1.1 Purpose

NASA's Kennedy Space Center (KSC) recently acquired two state-of-the-art wireless sensor systems as the final deliverable of a Phase II Small Business Technology Transfer (STTR) contract with Mnemonics, Inc. and the University of Central Florida (UCF), contract number NNX09CB69C. Mnemonics constructed the radio frequency (RF) interrogator portion of these systems and UCF constructed the sensors, which are based on a novel surface acoustic wave (SAW) architecture. The purpose of this testing is to characterize the performance of the system, both in its basic parameters and under a range of operating conditions.

### 1.2 Scope

NASA-funded development of SAW sensor technology is ongoing under a number of other STTR and Small Business Innovation Research (SBIR) contracts. The scope of this testing includes the sensor systems delivered to KSC under the above-referenced contract: two interrogator (transceiver) systems, Mnemonics part number 990-1139-001; four temperature sensors, with wooden mounting blocks; two antennas; two power supplies; network cables; and analysis software. Also included are a number of additional temperature sensors and newly-developed hydrogen sensors procured directly from UCF by KSC. One of the two interrogator systems was loaned to UCF to support their production of these additional sensors; thus the testing herein was primarily conducted with interrogator serial number 1, NASA ECN 2295445.

### 1.3 Reference Documents

The following documents form a part of this document to the extent specified herein.

| | |
|---|---|
| KNPR 8715.3 | KSC Safety Practices Procedural Requirements |
| TDL-0512 | Transducers Labs Laboratory Safety Manual |
| TDL-0516 | Transducer Development Laboratory Standard Cryogenic Operations and Test Set Up Reference Guide |
| TDL-0674-REF | Characterization Test Procedure for Surface Acoustic Wave (SAW) Hydrogen Sensors |
| Email dated 7 September 2011 | KSC 110009 – Conditional Radio Frequency Authorization for the SAW RFID Interrogator |

## 1.4 Data Handling

During testing, data was recorded by the test engineer on the data sheets included in the test procedure and in data log files. The data gathered during testing can be found in Appendix B.

## 2. TEST PROCEDURES AND ANALYSIS

### 2.1 Objectives

The objective of the testing herein is to characterize the electromagnetic compatibility (EMC) of the interrogator devices and quantify the performance of the sensor system as it is used to measure temperature and hydrogen concentration in various configurations.

### 2.2 Basic Characteristics

The SAW sensors (see Figure 1) are an assembly mounted on an FR-4 printed circuit board substrate, on which a folded dipole antenna pattern is laid out in copper. The sensor package, of similar size and shape to a dual in-line package (DIP) integrated circuit (IC), contains a lithium niobate ($LiNbO_3$) crystal which supports the SAW structures. The packaging design of the hydrogen sensors is similar to that of the temperature sensors; however, the hydrogen sensor package has an array of small holes to allow the sensor chip to be exposed to ambient hydrogen, while the temperature sensors have a solid cover.
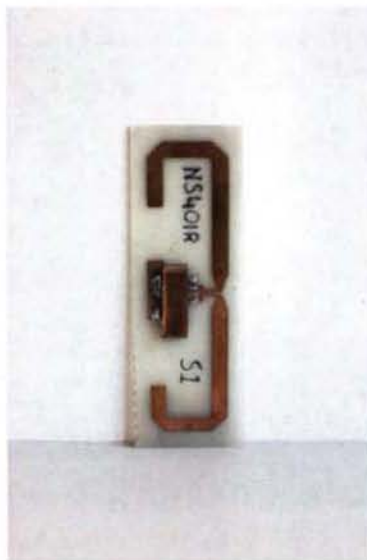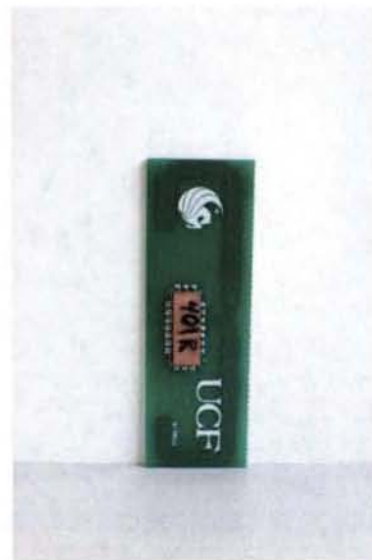


Supplied temperature sensor      Newly procured temperature sensor

**Figure 1.**    **SAW temperature sensors**

The SAW interrogator box (Figure 2) is a bench-top metal enclosure approximately 10 inches high by 4 inches tall by 8 inches deep. On one face of the box are three LED indicators: a green LED at the top lights solid when the power is on; a green LED in the center blinks when the system is operating correctly; and a red LED at the bottom indicates a fault. A momentary pushbutton resets the unit. There are also three electrical connections: an RJ45 is the primary Ethernet interface; a DB9 and an RJ11 are not documented and were not used in this testing. On the other face of the box are the vent for the cooling fan and four connections: a coaxial (barrel) connector for DC power; a female SMA connector for connecting the antenna; another female SMA connector used for Mnemonics' internal testing, not used here; and a pin-type connection (with ground lug) used as a trigger output. The supplied temperature measurement software runs in MATLAB with the Signal Processing Toolbox. For the temperature testing, a laboratory-assigned Dell Latitude E6500 with an Intel Core 2 Duo T9400 (2.53 GHz) processor and 2 GB of RAM with Windows XP Professional 32-bit was used to run the software. The hydrogen measurement software, procured from UCF along with the hydrogen sensors, is a compiled MATLAB application, and runs in the MATLAB Compiler Runtime environment. For the hydrogen testing, a laboratory-assigned Hewlett-Packard ProBook 6560b with an Intel Core i5-2520M (2.50 GHz) processor and 4 GB of RAM with Windows 7 Enterprise 64-bit was used to run the software.



Front view                    Back view
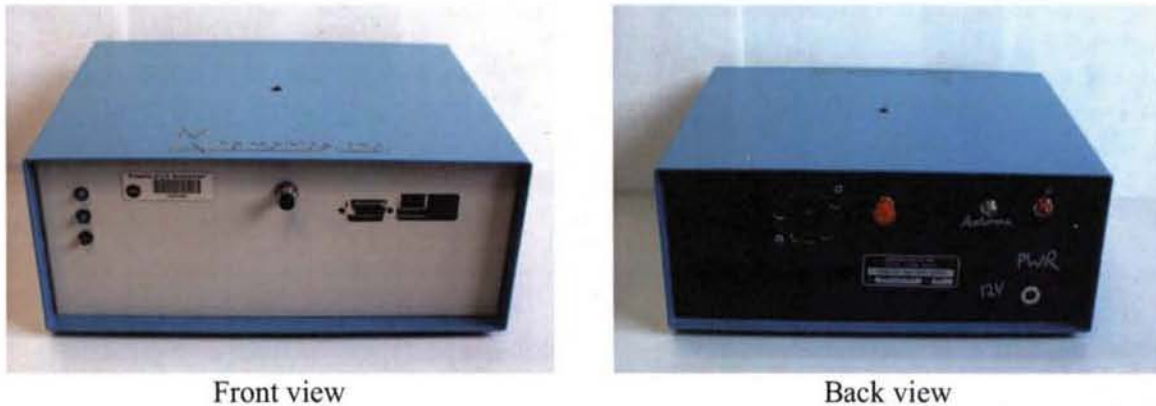
Figure 2.    RF interrogator box

When queried by the software, the interrogator sends out a stepped-frequency RF burst approximately 700 ns long, with 80 MHz of bandwidth centered at 915 MHz, having a nominal power of 3 W. This RF burst is received by the antenna on the sensor substrate, and a transducer excites a surface acoustic wave in the sensor crystal. This wave is reflected by a series of gratings called chips, and the reflected wave is converted back to an RF signal by the transducer. The RF signal is broadcast through the sensor antenna back to the interrogator antenna. The interrogator receives the RF signal from the sensor and mixes it down to a lower frequency, where it is digitized by a high-speed analog-to-digital converter (ADC). This data is transmitted over the Ethernet connection to the computer, which performs all the processing and analysis of the received signal to extract measurement data. The temperature sensors have one set of reflector chips, and the shift in reflected frequency is proportional to the temperature. The

hydrogen sensors have two sets of reflector chips; in the propagation path of one reflector is a hydrogen-sensitive film, which reduces the amplitude of the wave propagating in this path when exposed to hydrogen. The difference in amplitude between the two reflectors is given as an indication of hydrogen concentration. The shift in reflected frequency indicates the temperature, as with the temperature sensors; however, this capability shows significant offsets at room temperature, and was not tested further herein.

## 2.3    RF Characterization

Per the conditional KSC Radio Frequency Authorization (RFA) 110009, emissions characterization of the SAW interrogator was required before the system could be used outside the EMI test chamber. A simple test setup was constructed inside the chamber for this characterization. The interrogator itself was placed outside the chamber for easier access, and the antenna connection was routed through a type N bulkhead feedthrough on the chamber wall. The antenna was placed on the copper-surfaced test table inside the chamber, and one meter away was placed an ETS-Lindgren 3115 Double-Ridged Guide Antenna to receive the signal (see Figure 3). Two different pieces of test equipment were used to characterize the signal in this configuration: a high-speed digital oscilloscope, and a spectrum analyzer. In addition, near-field probe testing was conducted, using an EMC analyzer (specialized spectrum analyzer) to process the received signal.



**Figure 3.    RF characterization test setup**

Initial testing revealed difficulties in capturing the interrogator output on a spectrum analyzer. The output signal is nominally a stepped-frequency sine wave burst, 700 ns long, centered at 915 MHz, generated once per query by the operating software. The supplied version of the

operating software generated queries approximately once every ten seconds. Experimentation showed that the trigger signal output by the interrogator would be received after the start of the RF pulse, making it impossible to pre-trigger a spectrum analyzer using the provided trigger signal. Additionally, none of the available spectrum analyzers (see Table 1) had the capability to do a single-shot characterization of an RF pulse; all were of the swept-frequency type. An attempt to use the ETS-Lindgren FM5004 Field Monitor with an Amplifier Research FP2000 Isotropic Field Probe (see Table 2) gave no observable field measurement, likely because the effective duty cycle of the RF signal was so low.

**Table 1.        Available spectrum analyzers (as of 7 December 2011)**

| Spectrum Analyzer | Frequency Range |
|---|---|
| IFR Systems[1] 2390A Spectrum Analyzer | 9 kHz to 22 GHz |
| Agilent E7405A EMC Analyzer | 100 Hz to 26.5 GHz |
| Hewlett-Packard[2] 8568A Spectrum Analyzer | 100 Hz to 1.5 GHz |
| Agilent E4440A PSA Series Spectrum Analyzer | 3 Hz to 26.5 GHz |

**Table 2.        Available field probes (as of 12 December 2011)**

| Field Probe | Frequency Range |
|---|---|
| Amplifier Research FP2000 Isotropic Field Probe | 10 kHz to 1000 MHz |
| Amplifier Research FP2080 Isotropic Field Probe | 80 MHz to 40 GHz |
| ETS-Lindgren HI-4422 Isotropic Electric Field Probe | 10 kHz to 1000 MHz |
| ETS-Lindgren HI-6053 Isotropic Electric Field Probe | 10 MHz to 40 GHz |

### 2.3.1        Oscilloscope

*Test Method*

Given the limitations of the available spectrum analyzers, a Tektronix TDS5104B high-speed digital oscilloscope (see Table 3) was used to capture the received signal directly. The oscilloscope could be triggered on the rising edge of the RF signal, and has sufficient bandwidth and memory to capture the full length of the RF burst.

**Table 3.        Tektronix TDS5104B characteristics**

| | |
|---|---|
| Analog bandwidth | 1 GHz |
| Maximum sample rate | 5 GS/s |
| Metrology number | M88708 |
| Calibrated | 2 Sep 2011 |
| Calibration due | 2 Mar 2012 |
| Testing performed | 12-14 Sep 2011 |

---

[1] IFR Systems is now part of Aeroflex.

[2] Hewlett-Packard's test equipment business is now part of Agilent Technologies.

The oscilloscope was connected to the antenna directly via a coaxial cable, fed out of the EMI chamber using a bulkhead feedthrough. The trigger level was set above the ambient noise level, and configured for a single acquisition. This allowed the capture of the pulse in the time domain. In addition, the oscilloscope has a built-in FFT feature, which displays the calculated spectrum of the captured data. Multiple window (internal processing filter) types are available; two were used here: Gaussian and rectangular. Since the calculated spectrum was observed to vary somewhat from pulse to pulse, the oscilloscope was set to repetitive trigger, and the "infinite persistence" feature was used to overlay a series of spectra, giving an average envelope of the frequency content of the pulses.

*Data, Observations, and Analysis*

Figure 4 and Figure 5 show the leading and trailing edges, respectively, of the RF pulse as captured by the oscilloscope. Figure 6 gives the amplitude envelope of the pulse, using the local minima and maxima of the data. Note that this data is interpolated on the oscilloscope, improving the displayed resolution of the waveform but not the actual sampling rate; note also that the oscilloscope data has not been corrected for the effects of the antenna and cabling.
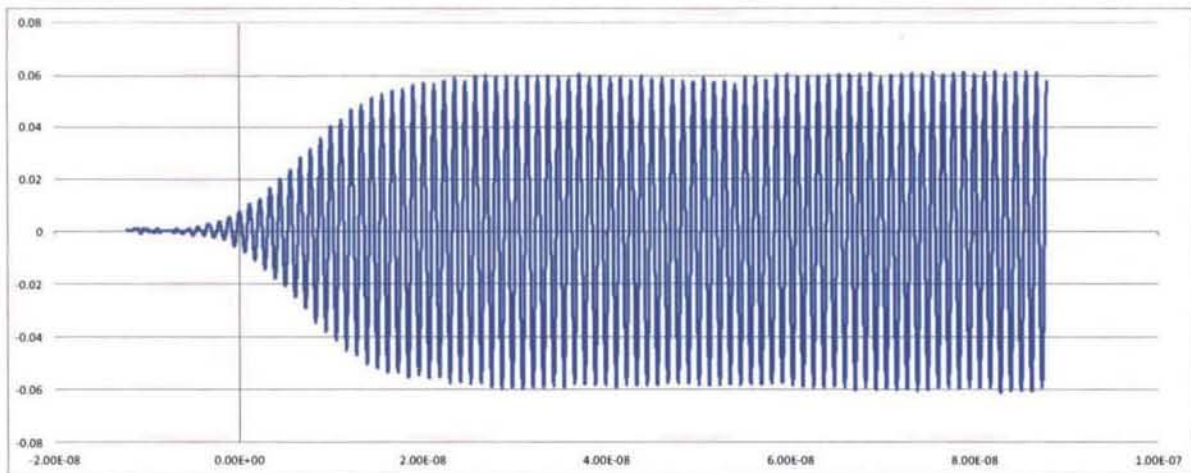


**Figure 4.** **Leading edge of RF pulse**

6
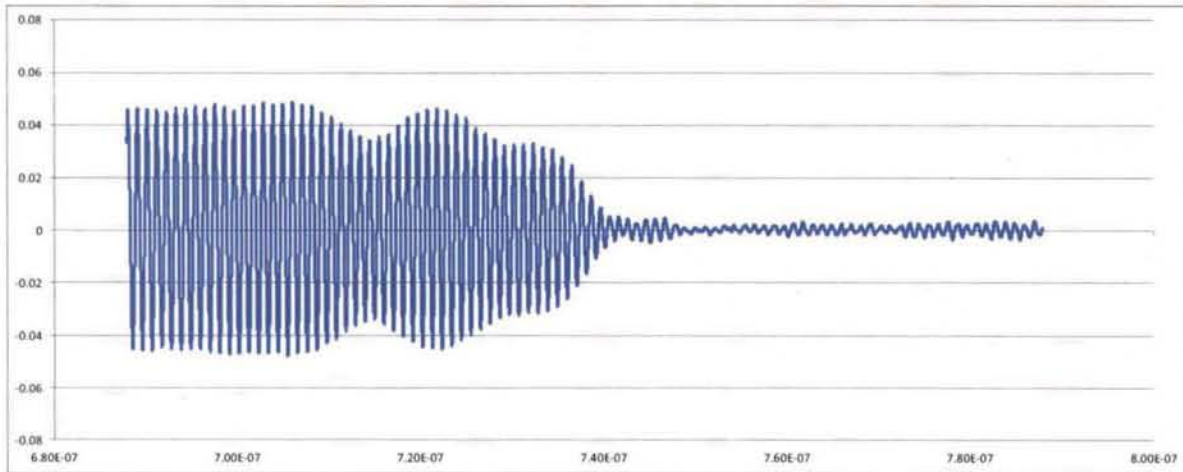
**Figure 5.    Trailing edge of RF pulse**
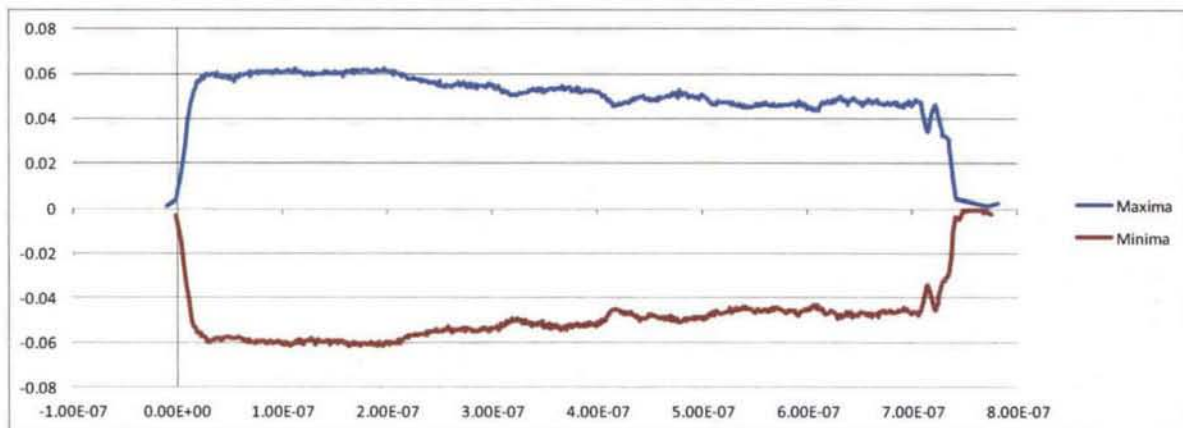


**Figure 6.    Amplitude envelope of RF pulse**

Figure 7 shows the overlaid spectra of approximately 100 pulses, processed using the FFT with a Gaussian window, showing a peak approximately 50 dB above the background noise level. Figure 8 shows a similar capture, processed using a rectangular window; this shows a peak roughly 47 dB above the background noise level.
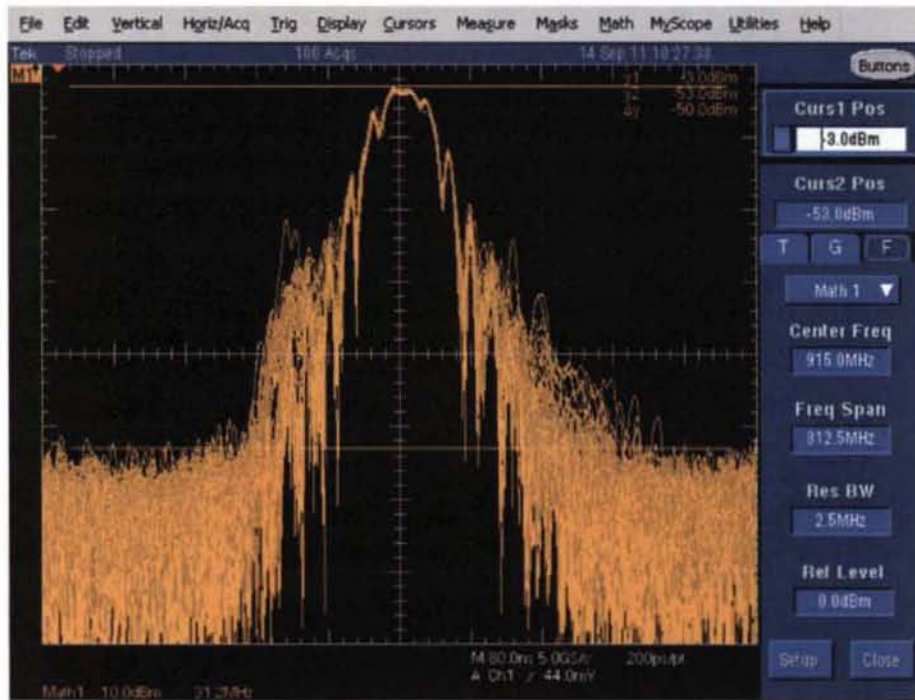
Figure 7.    Oscilloscope FFT, Gaussian window (approximately 100 pulses)
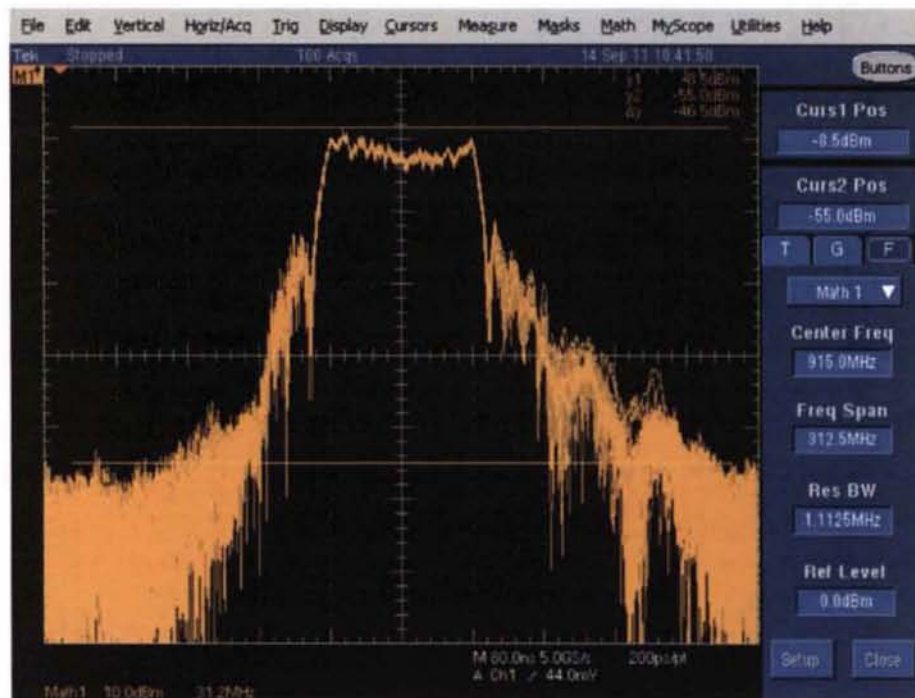


Figure 8.    Oscilloscope FFT, rectangular window (approximately 100 pulses)

### 2.3.2 Spectrum Analysis

Although the oscilloscope captures provide a thorough characterization of the fundamental pulse spectrum, the available analog bandwidth is 1 GHz, which does not allow the analysis of harmonics. Because the harmonics are critical to understanding the electromagnetic compatibility of the device, an alternate approach was developed, to use a spectrum analyzer in "max hold" mode (record the maximum observed value for a given period of time), and a long sample time to capture as many pulses as possible. The spectrum analyzer used for this testing was the Agilent E4440A; see Table 4 for details. Also in the signal path were the components listed in Table 5. These components were well-characterized for use in EMI pre-qualification testing in the laboratory, and their available correction factors were used to scale the data to the estimated electric field at the antenna position.

**Table 4.        Agilent E4440A characteristics**

| | |
|---|---|
| Bandwidth | 3 Hz to 26.5 GHz |
| Options | 111 USB Interface |
| | 115 Compact Flash Memory |
| | 239 EMC Analysis Application |
| Metrology number | M89632 |
| Calibrated | 14 Jul 2011 |
| Calibration due | 14 Jul 2012 |
| Testing performed | 14-22 Sep 2011 |

**Table 5.        Additional spectrum analysis components**

ETS-Lindgren 3115 Double-Ridged Guide Antenna
Agilent 87405C Preamplifier
Aeroflex/Weinschel attenuator
Cables

As a background reference, the spectrum analyzer was used to capture the spectrum of the EMI chamber with no operating devices inside. The captured spectrum for two hours, up to 3 GHz, is shown in Figure 9. Note two peaks in the background noise, which are thought to be RF signals impinging directly on the spectrum analyzer outside the chamber. The spectrum up to 5 GHz (Figure 10) shows similar interference peaks.

SCREN010.GIF                                    Run time: 2 hr

**Figure 9.        Spectrum of quiet EMI chamber to 3 GHz (raw data)[3]**

---

[3] Note that the assumption that the left peak is GSM-850 cell phone interference is supported by the narrowband spectrum corresponding to specific GSM uplink channels. Three closely spaced peaks are observable in the raw data: 826.5 MHz, close to GSM channels 139 and 140; 835.4 MHz, GSM channel 184; and 844.4 MHz, GSM channel 229.
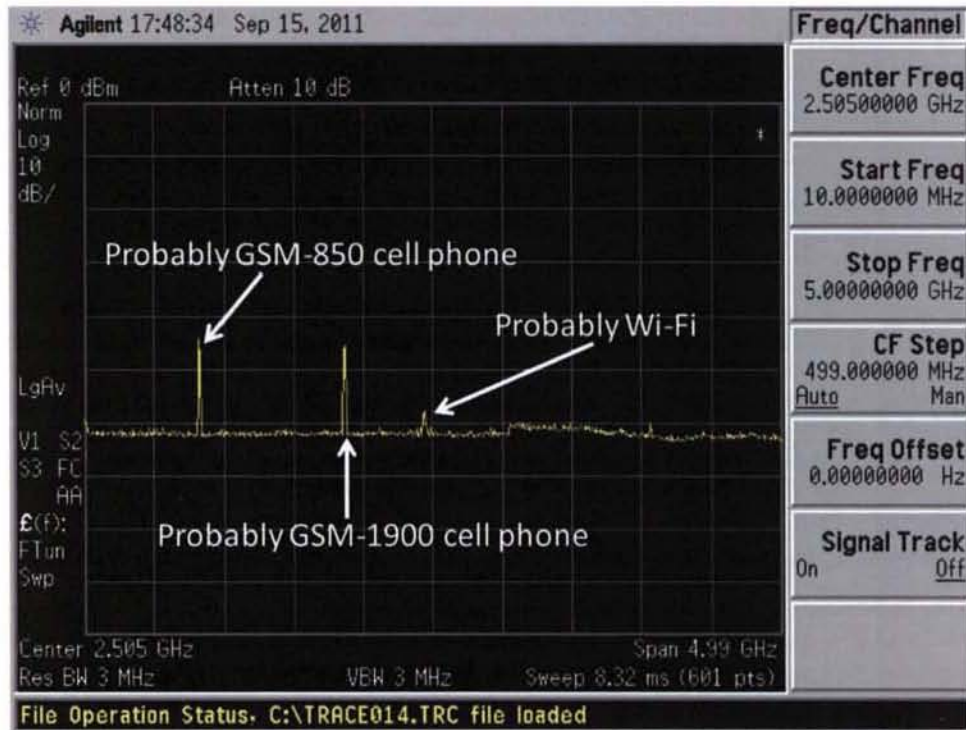
SCREN020.GIF                                                    Run time: 2 hr

**Figure 10.    Spectrum of quiet EMI chamber to 5 GHz (raw data)[4]**

### 2.3.2.1    Existing Software

*Test Method*

Using the existing UCF/Mnemonics software, the interrogator system was operated for approximately two hours with no sensors in the chamber, so that the output spectrum could be captured without influence from the sensors.

*Data, Observations, and Analysis*

The output spectrum of the interrogator up to 3 GHz, captured with the existing software, is shown in Figure 11. Note the small gaps in the spectrum of each harmonic, which indicates the sweep of the spectrum analyzer never captured a pulse in that frequency band. The small peak to the left of the third harmonic is thought to be IEEE 802.11b/g "Wi-Fi" (or another interference source in the ISM band). The output spectrum up to 5 GHz is shown in Figure 12; some peaks are visible in the fourth harmonic frequency band, but there are significant gaps in the spectra.

---

[4] Note that the assumption that the left two peaks are GSM cell phone interference is supported by the narrowband spectrum corresponding to specific GSM uplink channels. The peaks observable in the raw data are the following: 833.4 MHz, GSM channel 174; and 1872.9 MHz, close to GSM channels 625 and 626.

11
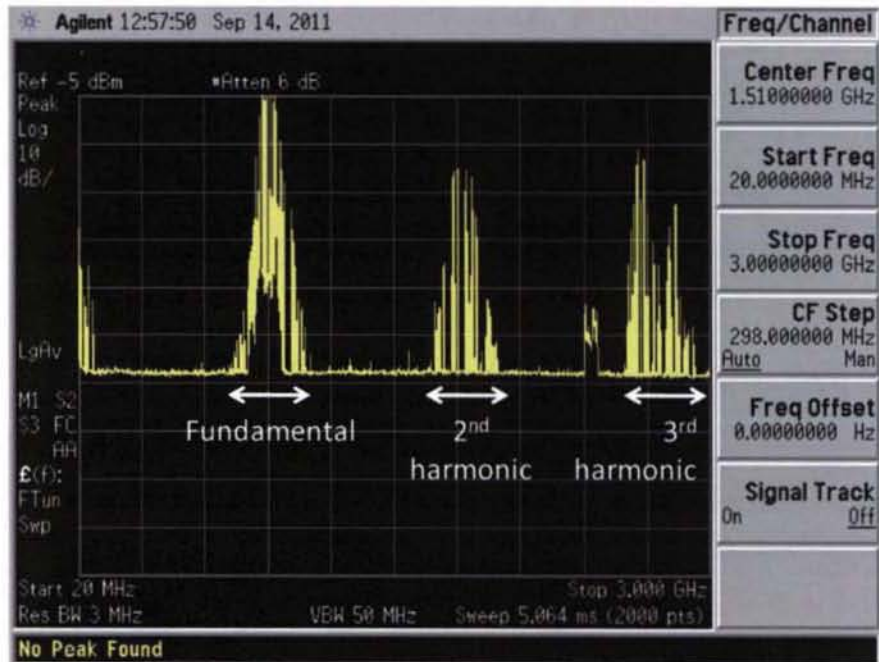
SCREN001.GIF                                                    Run time: 2 hr

**Figure 11.     Spectrum of interrogator to 3 GHz using existing software (raw data)**
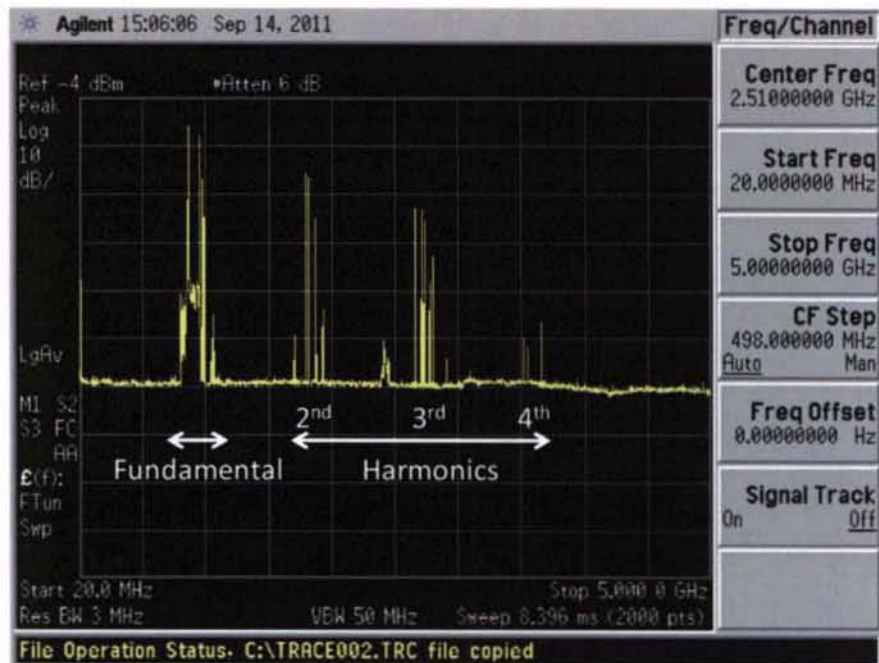


SCREN003.GIF                                                    Run time: 2 hr

**Figure 12.     Spectrum of interrogator to 5 GHz using existing software (raw data)**

### 2.3.2.2    Rapid Query Software

*Test Method*

Because the intermittent nature of the query signal leads to incomplete spectrum profiles, a MATLAB script was written to query the sensors more often, typically close to 8 times per second, without analyzing the received data; in the supplied software, the data analysis takes the vast majority of each query period. Using this script, more detailed spectra can be captured, since a given sweep of the spectrum analyzer has a greater chance of receiving an RF pulse.

*Data, Observations, and Analysis*

The following plots show the spectra captured using the rapid query script; each shows the full extent of the captured spectrum data. These plots have been corrected for the losses and gains in the RF path, as well as the antenna factor, to give a calculated value of the electric field at the receiving antenna. Figure 13 shows the interrogator spectrum out to 5 GHz; note that some peaks are visible as far out as the fifth harmonic. The noise floor curves upward with increasing frequency, primarily due to the characteristics of the cables and the antenna. Figure 14 shows a much narrower capture of the fundamental frequency band; data is not shown all the way to the left side (715 MHz) because those frequencies lie outside the antenna's design range. The upper blue trace is the spectrum when the interrogator is transmitting; the lower red trace is the spectrum when the interrogator is powered but idle (not transmitting). Note that the shape of the spectral profile compares well to that captured on the oscilloscope with the rectangular-window FFT (Figure 8). The peak value of the electric field in the fundamental band is 134 dBµV/m. Figure 15 shows the second harmonic spectrum, with a peak value of 114 dBµV/m, or about 20 dB below the fundamental. Figure 16 shows the third harmonic spectrum, with a peak value of 109 dBµV/m, or about 25 dB below the fundamental. The fourth harmonic spectrum is shown in Figure 17, with a peak value of 92 dBµV/m, or about 42 dB below the fundamental.
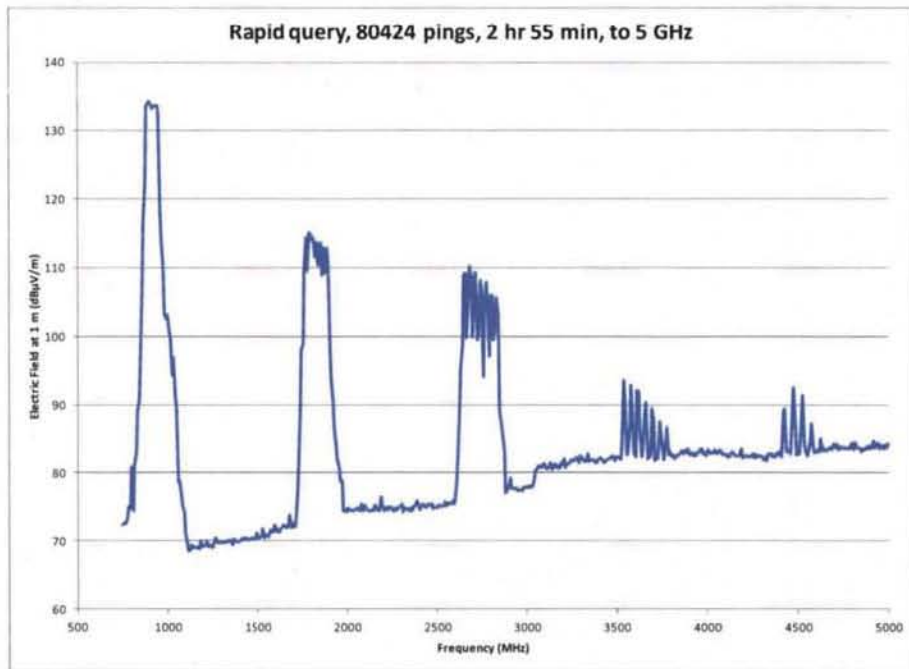
Figure 13.    Rapid query spectrum to 5 GHz
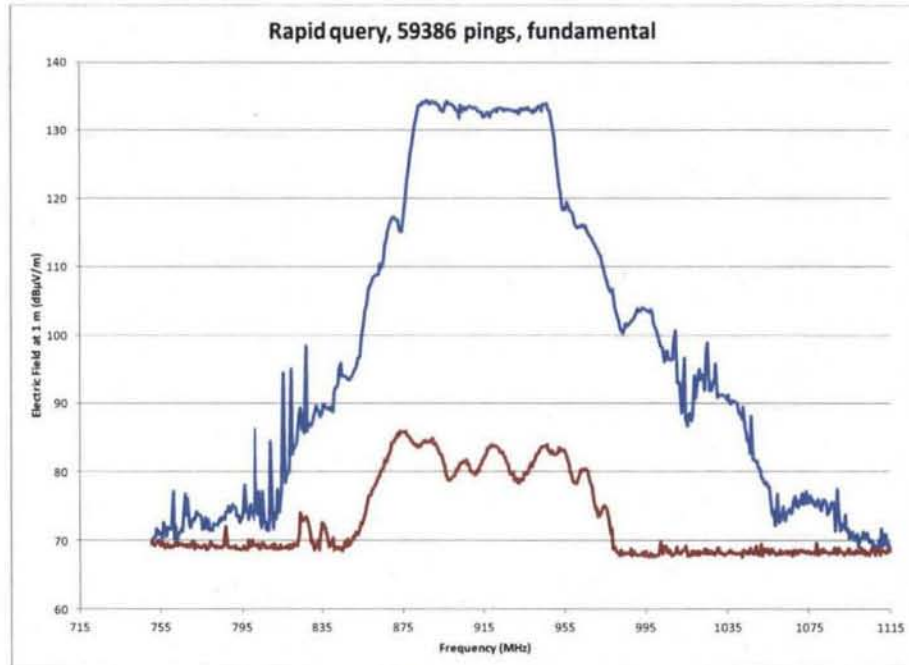


Figure 14.    Rapid query spectrum, fundamental frequency; blue trace: transmitting,
2 hr 8 min; red trace: idle, 1 hr 10 min
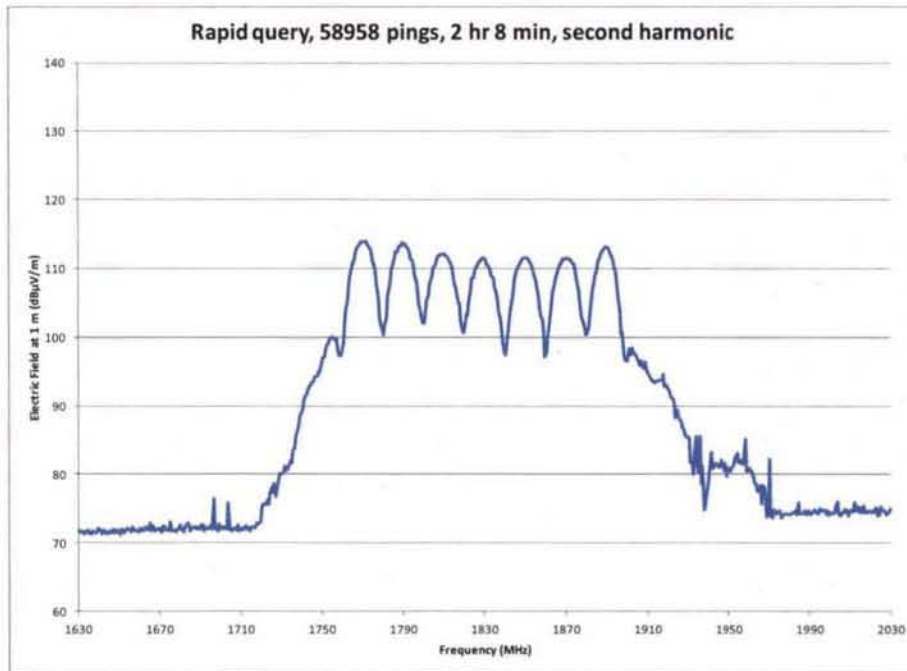
**Figure 15.    Rapid query spectrum, second harmonic frequency**
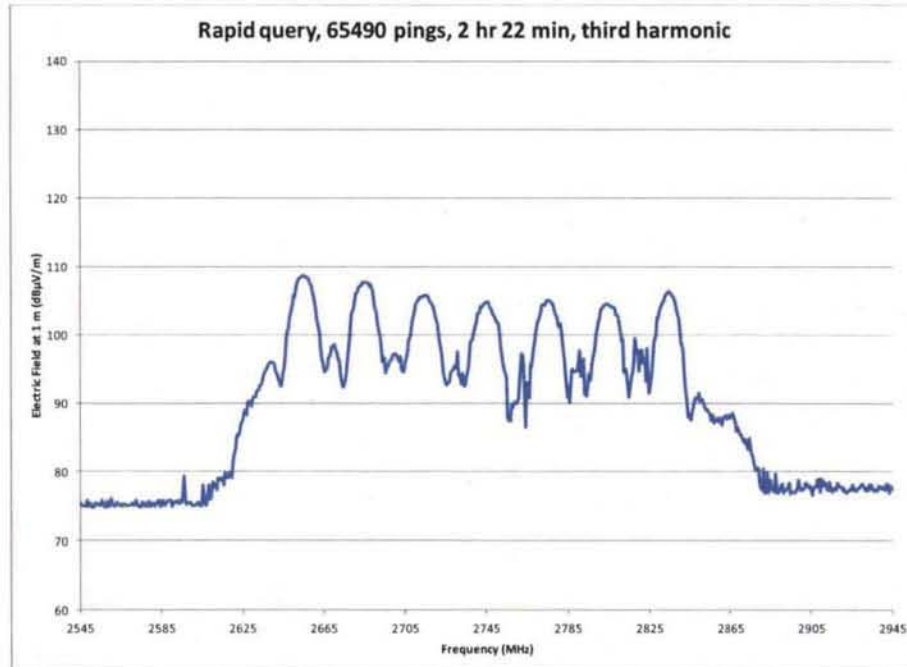


**Figure 16.    Rapid query spectrum, third harmonic frequency**
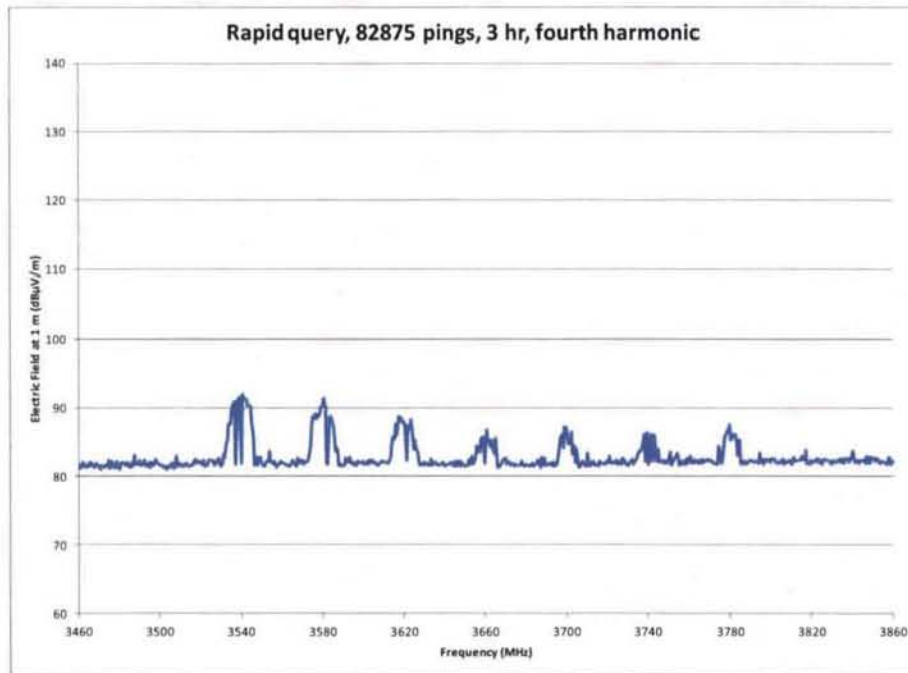
**Figure 17.    Rapid query spectrum, fourth harmonic frequency**

## 2.3.3    Near-field Probe

*Test Method*

To determine the radiated emissions characteristics of the interrogator box, a series of near-field probe tests were conducted. The cover of the box was removed, and data was collected near the various circuit components and cables. Details of the test equipment are listed in Table 6 and Table 7.

16

**Table 6.**    **Near-field probe calibrated test equipment**

Testing performed    10 Nov 2011
**Agilent E7405A EMC Analyzer**
Metrology number    M84901
Calibrated    08 Apr 2011
Calibration due    08 Apr 2012
Span setting    30 MHz to 1 GHz
RBW setting    120 kHz
VBW setting    300 kHz
Coupling setting    AC
Capture time    Max hold for 2.5 min
**Hewlett-Packard 8447F preamplifier**
Metrology number    M70131
Calibrated    14 Apr 2011
Calibration due    14 Jan 2012

**Table 7.**    **Near-field probe additional test equipment**

Agilent 11940A Near-field Probe
09-09-407 60" cable
08-08-801 39.7" cable

*Data, Observations, and Analysis*

The collected data is an extensive series of spectrum traces, and is available in Appendix A.

## 2.4    Temperature Sensor Performance

Following RF characterization, a series of tests was conducted to evaluate the performance of the system when measuring the supplied wireless temperature sensors.

### 2.4.1    Stability, Range, and Orientation

*Test Method*

Determining the accuracy of the system requires an understanding of the expected noise level. To characterize the stability and noise of the temperature measurement, a single sensor was placed on the test table inside the chamber along with the interrogator's antenna (Figure 18). A paper template marked increments of 0.25 m away from the antenna, with outlines for the sensor's wooden base to indicate a series of test orientations (see Figure 19; Figure 18 shows the sensor in orientation 1). The first four orientations were used for the initial testing. Orientations 5 and 6 were added to account for the third axis of rotation. Orientation 7 was added to test for ground plane effects (see Section 2.4.2).
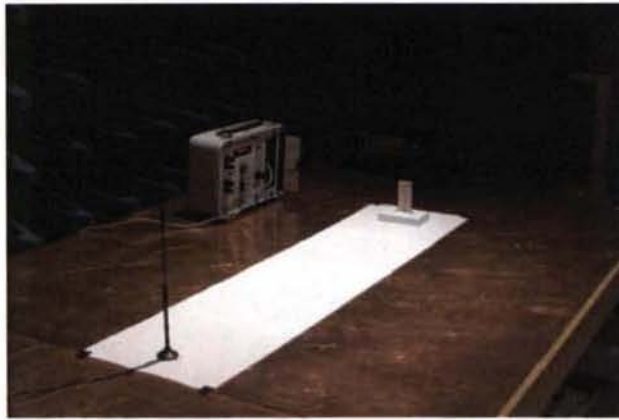
Figure 18.     Stability, range, and orientation test setup
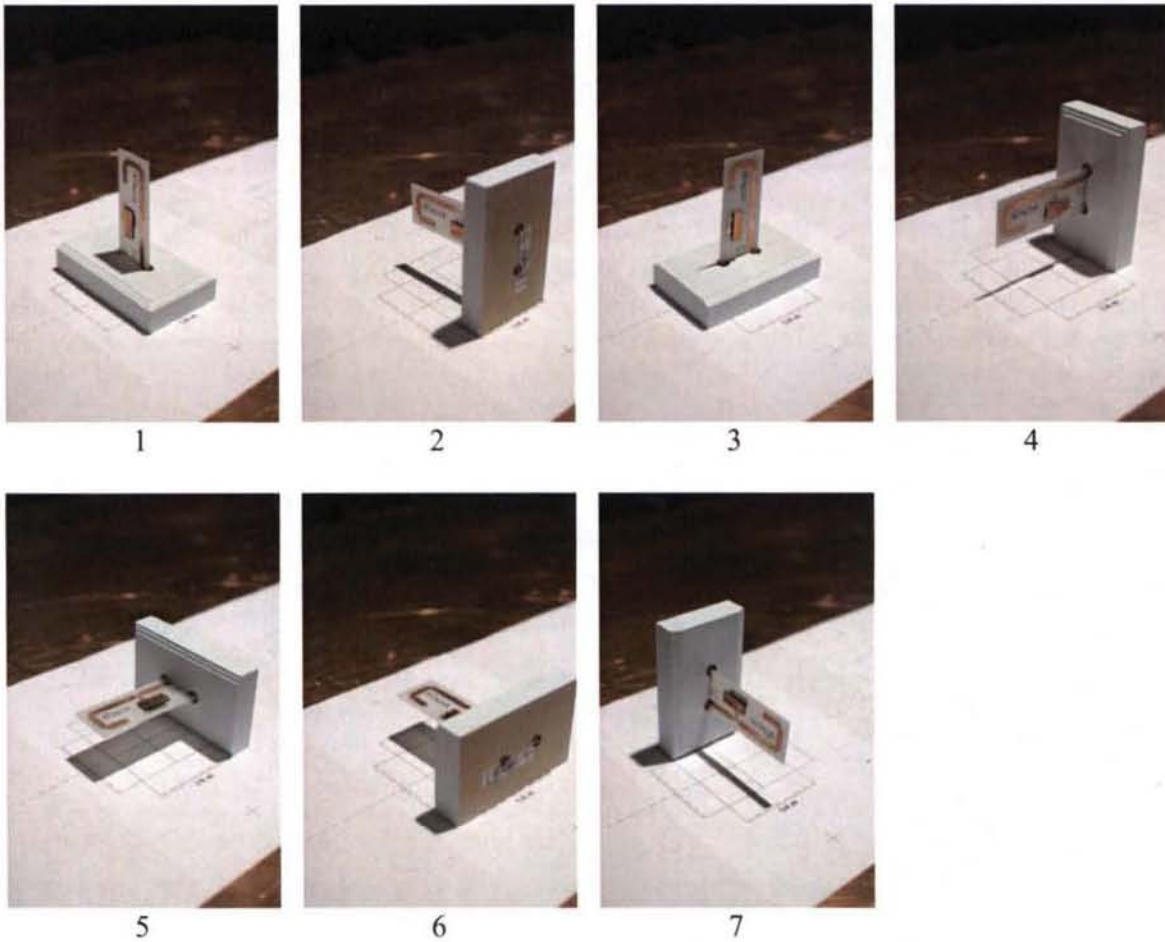


Figure 19.     Sensor test orientations

As the distance and orientation were varied, different levels of noise were observed in the measured temperature data. The operating software was modified to record the temperature data, the correlation peak (the software's internal measure of the signal strength), and the corresponding date and time to a text file for subsequent analysis. The display portion of the software was also modified to allow other software to be operated on the same computer, which was required for temperature testing. These changes resulted in improved speed, with data for a single sensor processed typically within four seconds, as a significant portion of the data processing time in the supplied software is spent updating the display. A sample data capture is shown in Figure 20.
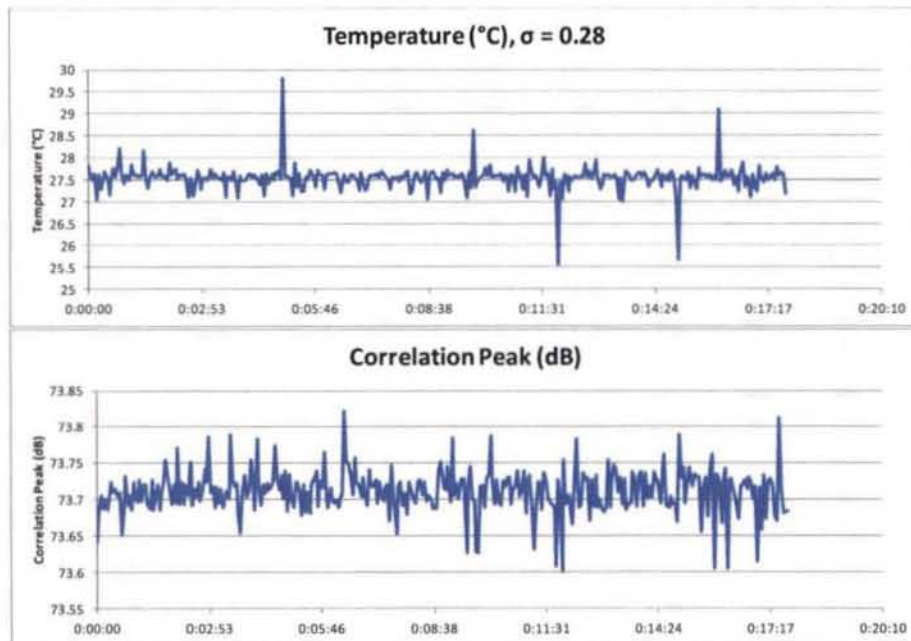


**Figure 20.    Sample data**

The standard deviation of the data was taken to be a reasonable measure of the noise level, given that the chamber temperature is reasonably stable over the time periods tested here. To confirm the stability of the room temperature, a thin foil thermocouple (Table 8) was attached to the back of one of the sensors using vinyl tape (Figure 21), and the temperature stability was observed during the data capture. Typical variation of the room temperature was no more than 0.2 °C, and the measured temperature was observed to vary slowly[5]. Thus the large excursions ("spikes") shown in the captured temperature data were taken to be errors rather than actual variation of the room temperature.

---

[5] These observations, for sensor NS402, were not recorded in the data sheets. Later, ambient temperature readings (with the thermocouple not attached to the sensor) were recorded at the beginning and end of the data captures.

**Table 8.      Temperature stability instrumentation**

**Omega Omni-Cal**
| | |
|---|---|
| Metrology number | M08216 |
| Calibrated | 01 Sep 2011 |
| Calibration due | 01 Feb 2012 |
| Testing performed | 5-12 Oct 2011 |

**Omega Cement-On Foil Thermocouple**
| | |
|---|---|
| Model number | CO1-T |
| Wire size | 30 gauge |
| Foil thickness | 0.0005 |
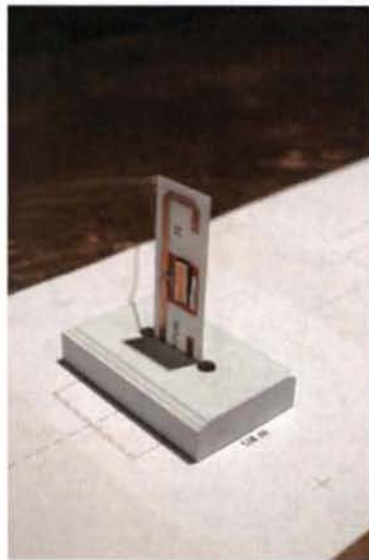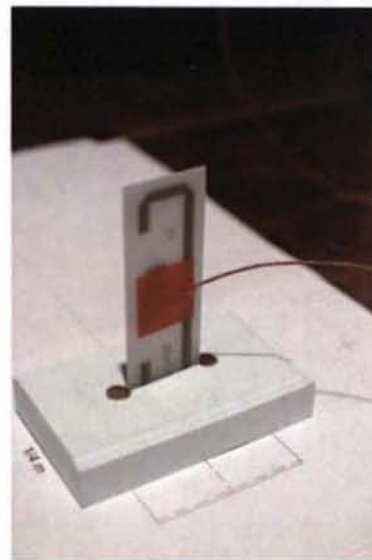


Front view                                    Back view

**Figure 21.      Thermocouple attachment for stability test (sensor NS402)**

*Data, Observations, and Analysis*

Noise performance was observed to vary significantly with sensor orientation (Figure 22). This was expected, since the interrogator antenna is a dipole and thus strongly polarization-dependent. The SAW sensor antenna is a folded dipole. Orientation 2, where the sensor was perpendicular to the antenna, was the worst overall. Orientations 5 and 6, where the sensor was parallel to the table, also performed poorly, but showed some improved performance at close range (Figure 23). Note that the testing matrix (see Appendix B) was not exhaustive in combinations of orientation and distance. It was also observed that the orientation dependence was different for the different sensors tested (Figure 24). For the four supplied sensors tested with one meter between the antenna and sensor, NS401R and NS404 showed the strongest orientation dependence, while NS402 was comparably insensitive to orientation. Orientation 7 was not tested in this dataset.
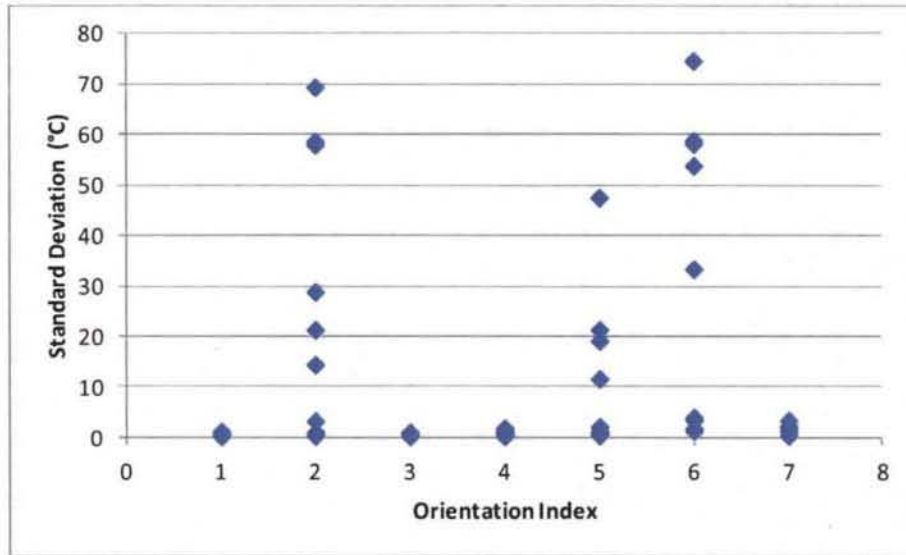
Figure 22.    Sensor noise vs. orientation; includes range/stability tests on table (71 runs)
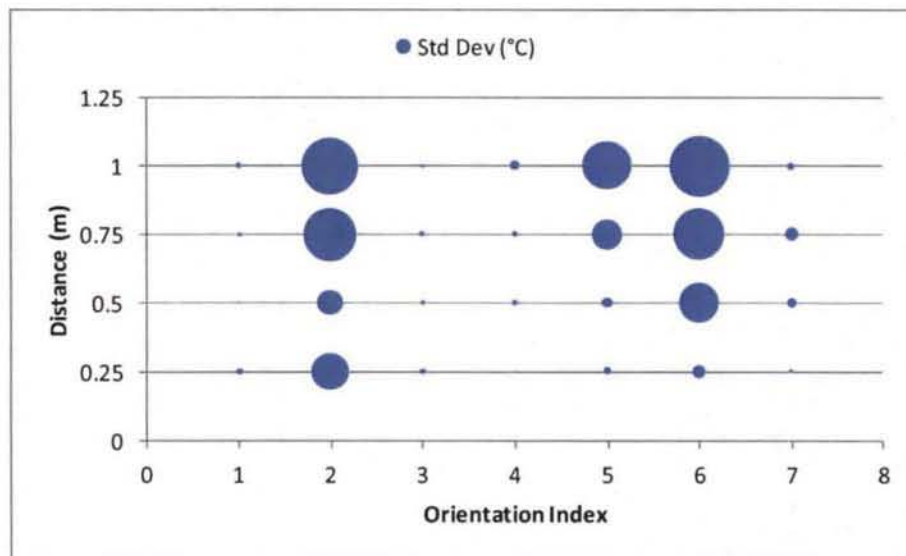


Figure 23.    Sensor noise vs. distance vs. orientation; includes range/stability tests on
table (71 runs)

21
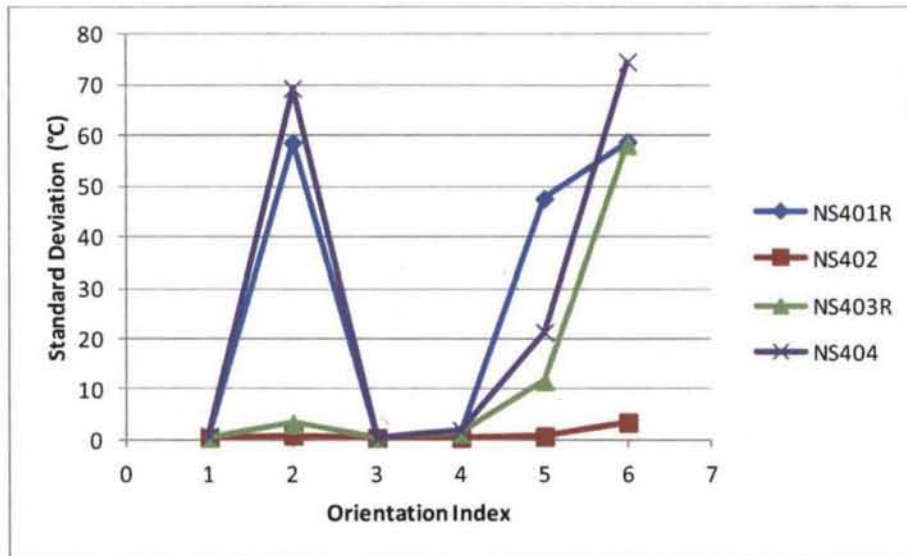
**Figure 24.** Sensor noise vs. orientation; includes range/stability tests at 1 m distance on table (24 runs)

### 2.4.2 Ground Plane Effects

*Test Method*

It was noted that the four supplied sensors were mounted in their wooden bases slightly differently: the vertical "arm" of the folded dipole structure was towards the left on the even-numbered sensors NS402 (see Figure 21) and NS404, but towards the right on the odd-numbered sensors NS401R (see Figure 19) and NS403R. This was not intentional, and not expected to significantly affect the performance for some orientations (1, 3, and 5), but could affect the performance of the orientations where this discrepancy changed the distance between the vertical arm of the dipole and the surface of the table, which is a large ground plane. To determine the significance of this effect, results from orientation 2 were compared to orientation 7, which simulates the difference between the left- and right-handed mounting.

*Data, Observations, and Analysis*

A sample data comparison is shown in Figure 25, showing a vast difference in performance between the two orientations. For sensor NS404 with one meter between the antenna and sensor, orientation 2 produced no useable data (standard deviation of 69.3 °C), but orientation 7 produced reasonably good data with a standard deviation of 1.2 °C. Thus ground plane effects must be considered with this system design, and future testing should ensure consistent mounting orientation of the sensors.

Orientation 2          Orientation 7
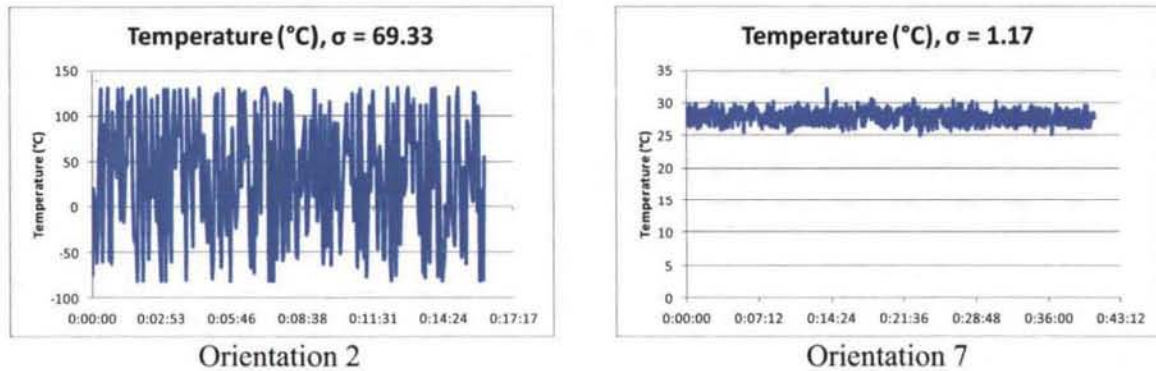
**Figure 25.    Ground plane sensitivity results (range/stability, table, NS404, 1 m)**

## 2.4.3    Free-Space Range

*Test Method*

In addition to the testing on the copper-surfaced table in the EMI chamber, a series of free-space tests were conducted to characterize the maximum usable range of the sensors. To reduce ground plane effects, the interrogator antenna and sensor were mounted on separate plastic tripods (Figure 26), and moved the maximum available distance apart along the diagonal of the chamber. Temperature data was collected, and the sensor tripod was moved closer to the interrogator antenna; this was repeated several times. At each test distance, the sensor was visually aligned facing the interrogator antenna.



Interrogator antenna          Sensor

**Figure 26.    Free-space range setup**

23

*Data, Observations, and Analysis*

A summary chart of the free-space testing is shown in Figure 27. Note the clear threshold between 4 m and 5 m, which may also be seen in the sample data charts in Figure 28. Beyond 4 m, it would be difficult to recover useable data; at 4 m and less separation, a clear trend is visible, with a decreasing noise band as the separation distance is decreased.
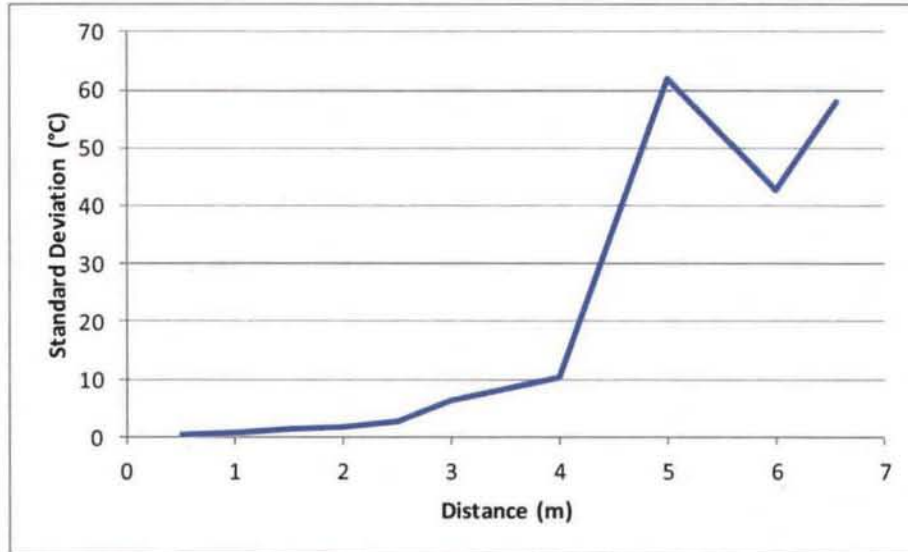


**Figure 27.     Free-space testing results summary; NS401R and provided antenna mounted on plastic tripods**
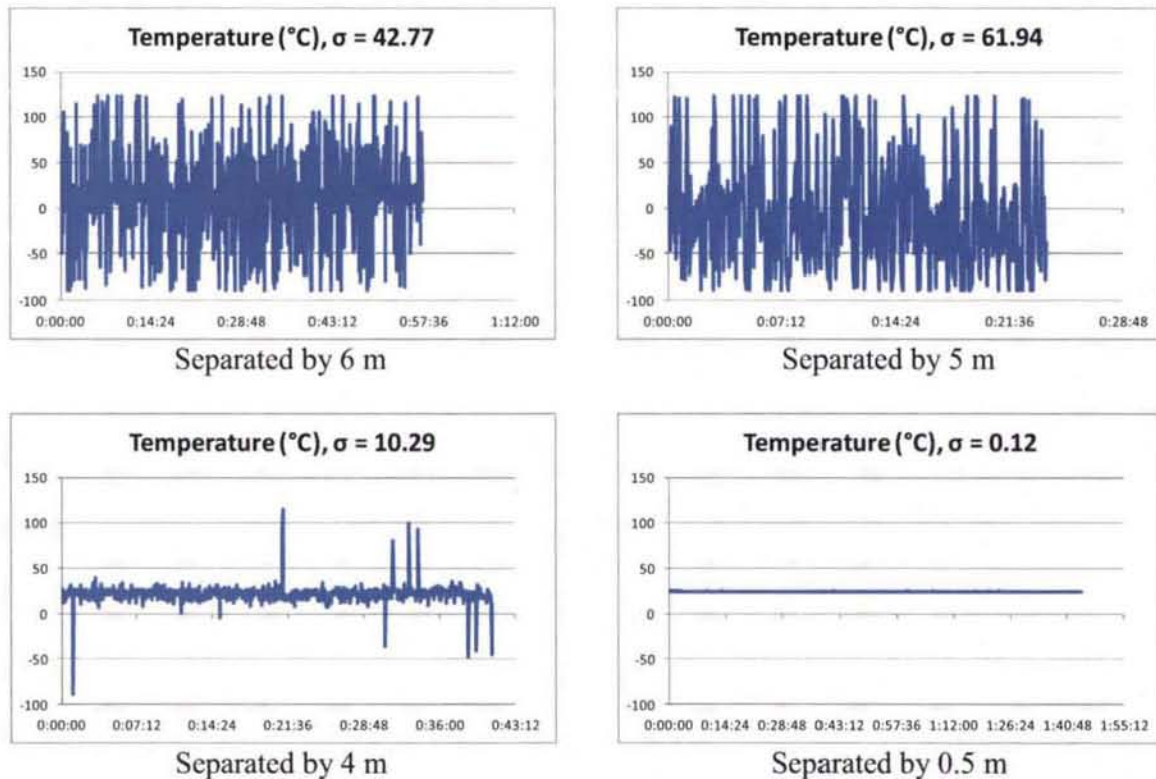
**Figure 28.    Free-space testing sample results; NS401R and provided antenna mounted on plastic tripods**

### 2.4.4    Aggregate Results

*Test Method*

One challenge noted during testing is that the operating software may produce rapidly varying results if the signal level is low. This is because the software makes no attempt to determine whether a given sensor is present or producing useful data; rather, it determines the best correlation of the received signal with the expected sensor response, and reports this correlation as the result. The strength of the correlation is measured in the software as the "correlation peak" (in dB). To determine whether this would be a useful measure of data quality, the results of the testing in Sections 2.4.1 through 2.4.3 were plotted as the standard deviation of the temperature measurement versus the correlation peak.

*Data, Observations, and Analysis*

Results of this analysis are shown in Figure 29; a detailed view of the lower-right portion of the chart is shown in Figure 30. The standard deviation of the data increases smoothly below 55 dB correlation peak, then increases rapidly below 40 dB. This should make it possible to give a reasonable confidence interval on a given measurement based on the value of the correlation

peak. Because this measurement process is considered to be coherent, it may also be possible to dynamically adjust the integration time to improve results when the correlation peak is low.
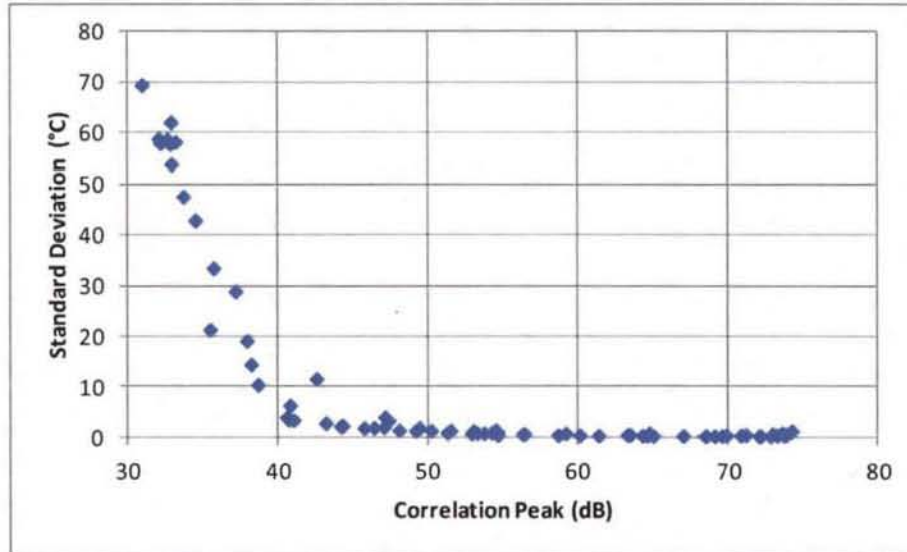


Figure 29.  Sensor noise vs. signal; all range/stability data with correlation peak included (77 runs)
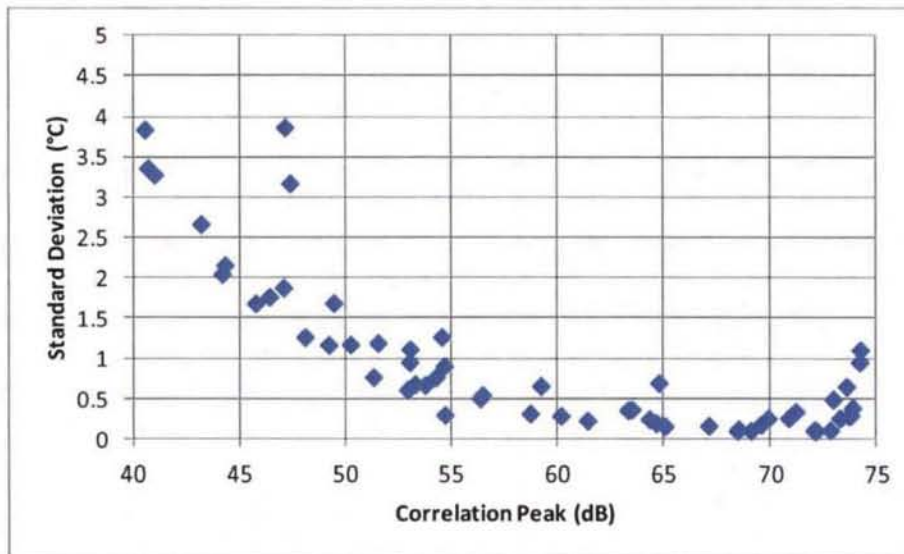


Figure 30.  Sensor noise vs. signal (detailed view); all range/stability data with correlation peak included (77 runs, 60 shown here)

### 2.4.5    Temperature Performance

*Test Method*

To characterize the temperature performance of the SAW sensors, a test setup was developed to expose the sensors to a controlled temperature environment while maintaining an RF path to the interrogator antenna. Placing the antenna inside an existing temperature chamber proved to be impractical, since the antenna height was greater than the available inside height of the chamber, and since the achievable distance from the antenna to the sensor was very limited. Instead, the sensor was placed directly behind the chamber window, and the interrogator antenna was mounted on a plastic tripod one meter away (Figure 31). This proved to give good signal levels while allowing flexibility in the antenna placement. To measure the temperature of the sensor, a Type T thermocouple was clamped to the substrate of the sensor, and wired to a Keithley 2002 multimeter equipped with a thermocouple scan card (Table 9). The environmental chamber, a Sun Electronic Systems EC12 (Table 10), uses liquid nitrogen for cooling and a resistive element for electric heating. Steps were taken to maximize safe operations, including setting up the liquid nitrogen supply cylinder and nitrogen exhaust vent outside the EMI chamber. Because liquid nitrogen had not been previously used inside the EMI chamber, this configuration required additional Safety review. To demonstrate the feasibility of the general approach, the chamber was tested in heat-only mode, which does not require liquid nitrogen. To cool the chamber, an ebm-papst 8218J/2H4 fan was attached to the side of the chamber, facing into the side feedthrough port. This fan was powered by an Agilent E3645A DC power supply.



Overview                                        Sensor

**Figure 31.     Temperature test setup, initial version**

The RF power levels broadcast by the interrogator are above that generally recognized as safe for personnel to be inside the EMI chamber, thus the whole test setup had to be remotely operated.

The Sun chamber, Agilent power supply, and Keithley multimeter all have GPIB interfaces, and this presented the best option for control and monitoring. A Hewlett-Packard 37203A HP-IB extender (HP-IB is compatible with GPIB) was placed in the chamber and cabled to the test equipment; the coaxial connection was connected to a bulkhead feedthrough on the chamber wall. This was then connected to a second extender outside the chamber. This allowed the laptop and its GPIB interface to interface with the test equipment. An existing LabVIEW virtual instrument was available to monitor the Keithley multimeter, but new virtual instruments had to be developed to control the Sun chamber and Agilent power supply. All three were capable of running simultaneously with the MATLAB-based SAW sensor operating software.

**Table 9.      Calibrated instrumentation for temperature test**

| | |
|---|---|
| Testing performed | 19 Oct 2011 |
| **Keithley 2002** | |
| Metrology number | M66382 |
| Calibrated | 10 Jun 2011 |
| Calibration due | 10 Nov 2011 |
| **Keithley 2001-TCSCAN** | |
| Metrology number | M71628 |
| Calibrated | 10 Jun 2011 |
| Calibration due | 10 Feb 2012 |

**Table 10.      Additional equipment for temperature test**

Sun Electronic Systems EC12 test chamber
Two, Hewlett-Packard 37203A HP-IB extenders
National Instruments PCMCIA-GPIB interface card
Type T thermocouple (soldered from wire)
ebm-papst 8218J/2H4 fan
Agilent E3645A DC power supply
Irwin Quick-Grip 1½" – 38 mm clamp

*Data, Observations, and Analysis*

Initial temperature test results are shown in Figure 32. Note that the SAW sensor measurement tracks well with the thermocouple measurement, but with an error which appears to increase as temperature increases. This may reflect an error in the assumed temperature coefficient of the SAW sensor, −94 ppm/°C. Further testing, with extended temperature ranges, may be conducted with future task order funding, pending Safety approval, and once an improved sensor mount is constructed.
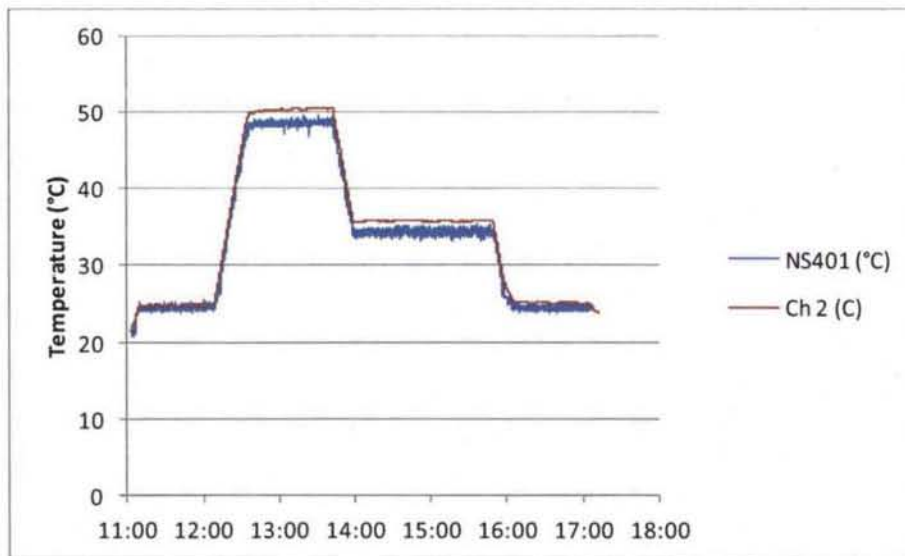
**Figure 32.** **Temperature test results; blue trace: SAW sensor; red trace: thermocouple**

### 2.4.6 Additional Sensors

A set of eight additional temperature sensors (two each of four codes) were ordered as part of this testing; these sensors were received from UCF on 16 November 2011, and will be tested if future task order funding permits.

### 2.5 Hydrogen Sensor Performance

A set of four hydrogen sensors was ordered from UCF; these sensors were received on 23 November 2012. Sensor serial numbers are listed in Table 11. Sensor BHF401-062712 was damaged in handling in the lab before testing could be conducted; it has since been returned to UCF for possible repair. Sensors are referred to in the testing herein by their code number (e.g., BHF401) without the date of manufacture.

**Table 11.** **Hydrogen sensor serial numbers**

BHF401-062712
BHF402-052312
BHF403-052312
BHF404-052312

### 2.5.1 Hydrogen Test Setup

Testing of hydrogen sensors, as well as testing for effects of local ambient pressure, requires a pressure enclosure for the sensors. This enclosure must be capable of safely withstanding test pressures, yet must pass the RF signals of the interrogator and sensor. Various materials were

researched for this purpose; options included a sight glass or chemical reaction vessel, but these proved to be too expensive for the available funding. An enclosure primarily constructed of plastic pipe was considered a good, less expensive option. Though it is reasonably available and inexpensive, clear PVC tubing was rejected because PVC is not considered safe for compressed gas service. This is due to the failure mode of PVC, brittle fracture, which may produce shrapnel. Market research found two plastic piping systems which are specifically designed for compressed gas service: Asahi America Air-Pro (HDPE) and IPEX Duraplus Air-Line (ABS). Duraplus Air-Line was preferable for this testing since it may be assembled via solvent welding, without the purchase or rental of additional equipment. The solvent and cleaner both use methyl ethyl ketone (MEK), which required Safety approval; its use was approved outdoors, away from facility entrances, with nitrile gloves preferable for handling. The upper part of the pressure enclosure consists of a cap, a section of tubing, and a stub socket flange. This section is secured using a steel backing plate around the stub flange, bolted through to an aluminum base, trapping a gasket for sealing the enclosure. This assembly allows the RF signals to pass through while allowing service up to 150 psi with good safety margin; the piping system is rated up to 185 psi continuous service at room temperature. All testing performed thus far has been with the downstream port of the last test fixture open to the room, thus the actual internal pressure is quite low. One of the completed fixtures is shown in Figure 33.



Overview                                        Sensor mounted in fixture

**Figure 33.    Hydrogen test fixture**

Five compressed gas cylinders from local stock were used for the testing herein; the commodities are listed in Table 12. Details of the calibrated and uncalibrated test equipment are shown in Table 13 and Table 14, respectively.

Table 12.    Commodities used for hydrogen testing

| Commodity | Actual Contents |
|---|---|
| Breathing air | Breathing air |
| 2% hydrogen in air | 2.01% hydrogen, balance air |
| 3% hydrogen in air | 3.02% hydrogen, balance air |
| 50% helium, 50% air | 62.6% helium, 37.4% air |
| 2% hydrogen in nitrogen | 2.00% hydrogen, balance nitrogen |

Table 13.    Calibrated test equipment for hydrogen testing

Testing performed    24 Jan-20 Feb 2013
**CalTechnix[6] molbox1**
Metrology number    M70271
Calibrated    11 Oct 2012
Calibration due    11 Oct 2013
**DH Instruments[7] molbloc 30 slm-SWG-V-Q**
Metrology number    M70269
Calibrated    11 Oct 2012
Calibration due    11 Oct 2013
**DH Instruments molbloc 1 slm-SWG-V-Q**
Metrology number    M70268
Calibrated    11 Oct 2012
Calibration due    11 Oct 2013
**Fluke 8840A Multimeter**
Metrology number    M07563
Calibrated    17 Jul 2012
Calibration due    17 Mar 2013
**Yokogawa 7651 Programmable DC Source**
Metrology number    M89084
Calibrated    31 Oct 2012
Calibration due    30 Sep 2013

---

[6] The molbox series is now produced and supported by Fluke Calibration.
[7] DH Instruments is now part of Fluke Calibration.

**Table 14.    Additional test equipment for hydrogen testing**

**Mnemonics, Inc. model 990-1139-001 SAW Transceiver System**
Serial number          001
**Sierra Instruments C100L-DD-4-OV1-SV1-PV2-V1-S0-C0-GS-CC**
Serial number          106456
Range                  10 SLPM
**Sierra Instruments C100L-DD-4-OV1-SV1-PV2-V1-S0-C0-GS-CC**
Serial number          106457
Range                  10 SLPM
**MKS Instruments M100B01313CR1BV**
Serial number          021578273
Range                  1000 SCCM N2
**Agilent E3631A DC Power Supply**
Serial number          MY40040115
**Whitey (now Swagelok) SS-44XF4 3-Way Valve**

### 2.5.2    Baseline and Range

Initial testing was performed to determine the noise level of the sensors when exposed to ambient air, both with the sensors spaced 90° apart and with them close together. The test enclosures were installed on the test fixtures, but no compressed gas supply was used. For each test, the test fixture was oriented with the sensor element above the inlet port, facing the Interrogator antenna (see Figure 34). The test table in the large EMI chamber is approximately 1.2 m by 4 m, which supports tests with the sensors spaced 90 degrees apart at a distance of 0.5 m, as well as tests with the sensors close together at distances up to approximately 3.5 m, as shown in Figure 35; tests were conducted up to 3 m, as shown in Figure 36.
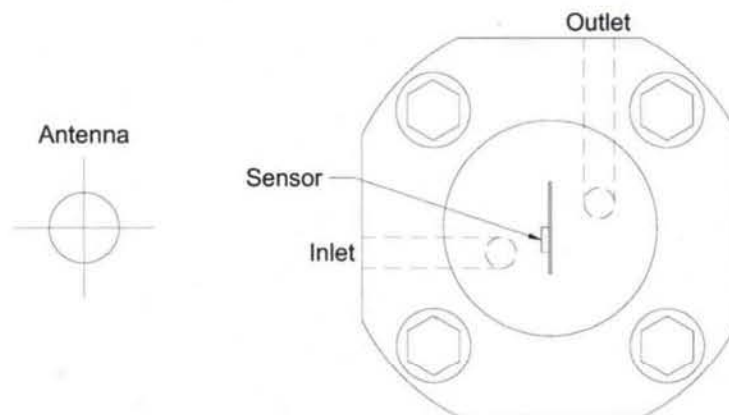


**Figure 34.    Test fixture orientation (details omitted for clarity)**
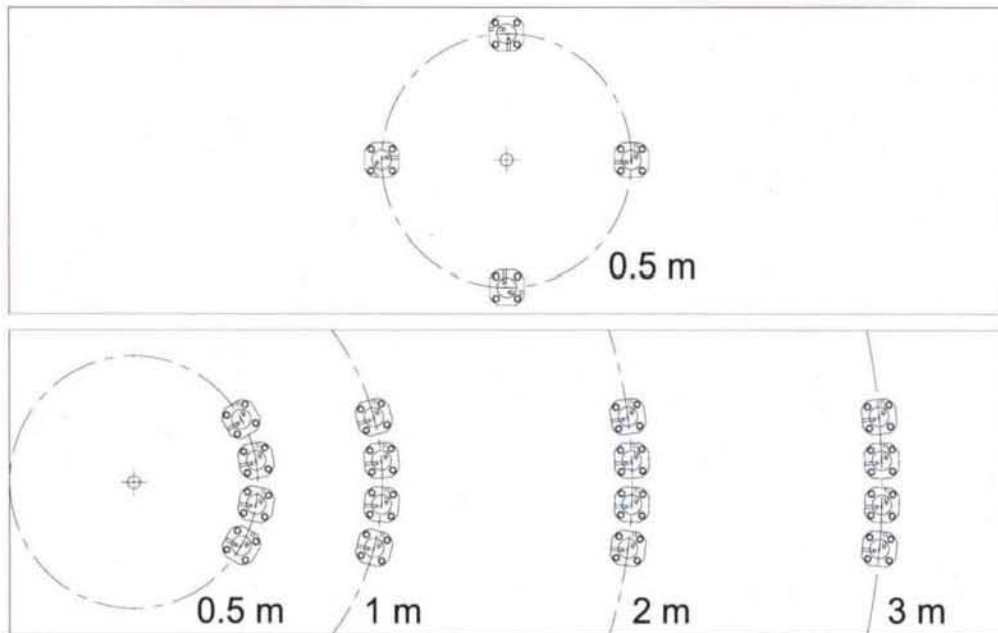
**Figure 35.     Baseline and range test arrangements, large chamber**



**Figure 36.     Range test overview; 3 m test shown**

Initial baseline testing showed that, at a distance of 0.5 m, both the 90° arrangement and the closely spaced arrangement had low levels of noise; see Figure 37 and Table 15. Sensors BHF402 and BHF404 had higher levels of noise in the close arrangement, while BHF403 had a higher level of noise in the 90° arrangement.
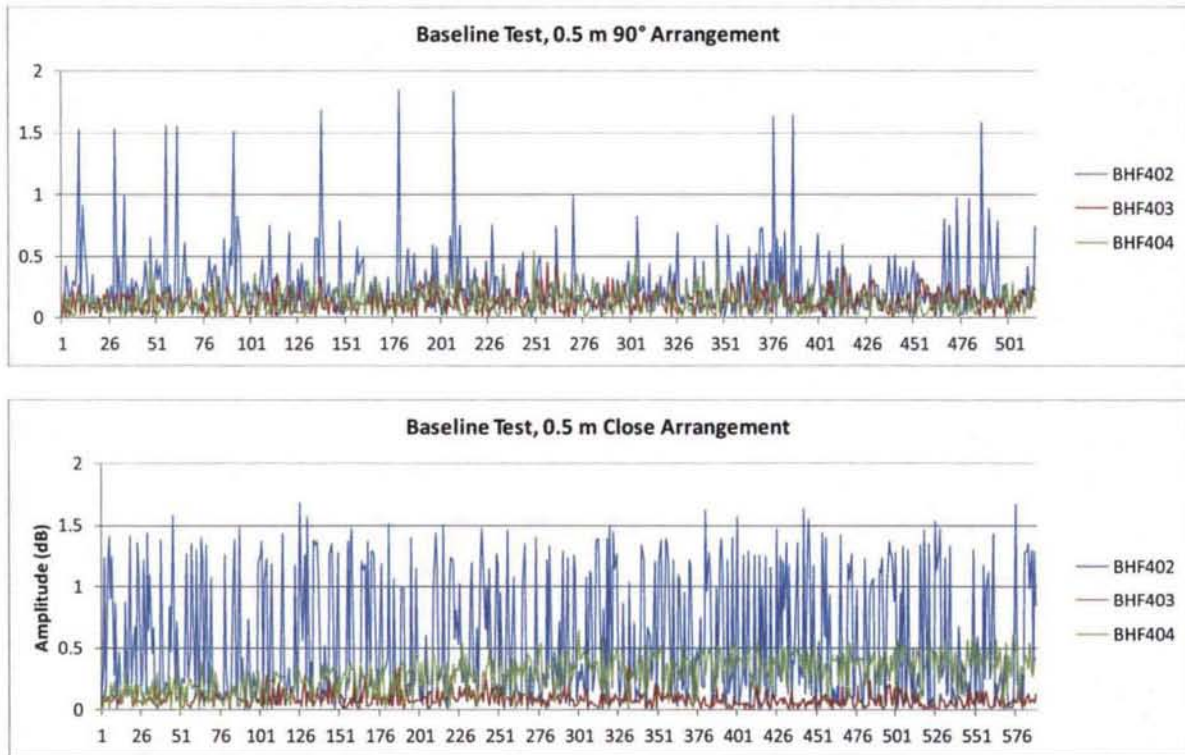


**Figure 37.    Baseline test results**

Range testing was conducted with the sensors in the closely spaced arrangement, given the available space on the test table. Sensor noise increased with increasing distance, with one exception: sensor BHF402 had lower noise at 2 m than at 1 m; see Figure 38 and Table 15.

**Table 15.    Baseline and range test summary**

| Distance (m) | Arrangement | Average (dB) | | | Standard Deviation (dB) | | |
|---|---|---|---|---|---|---|---|
| | | **BHF402** | **BHF403** | **BHF404** | **BHF402** | **BHF403** | **BHF404** |
| 0.5 | 90° | 0.254 | 0.132 | 0.125 | 0.282 | 0.086 | 0.095 |
| 0.5 | Close | 0.550 | 0.082 | 0.287 | 0.515 | 0.059 | 0.144 |
| 1 | Close | 1.129 | 0.156 | 0.316 | 0.794 | 0.112 | 0.191 |
| 2 | Close | 1.047 | 0.618 | 0.368 | 0.541 | 0.435 | 0.276 |
| 3 | Close | 1.408 | 2.573 | 2.428 | 0.943 | 1.561 | 0.957 |
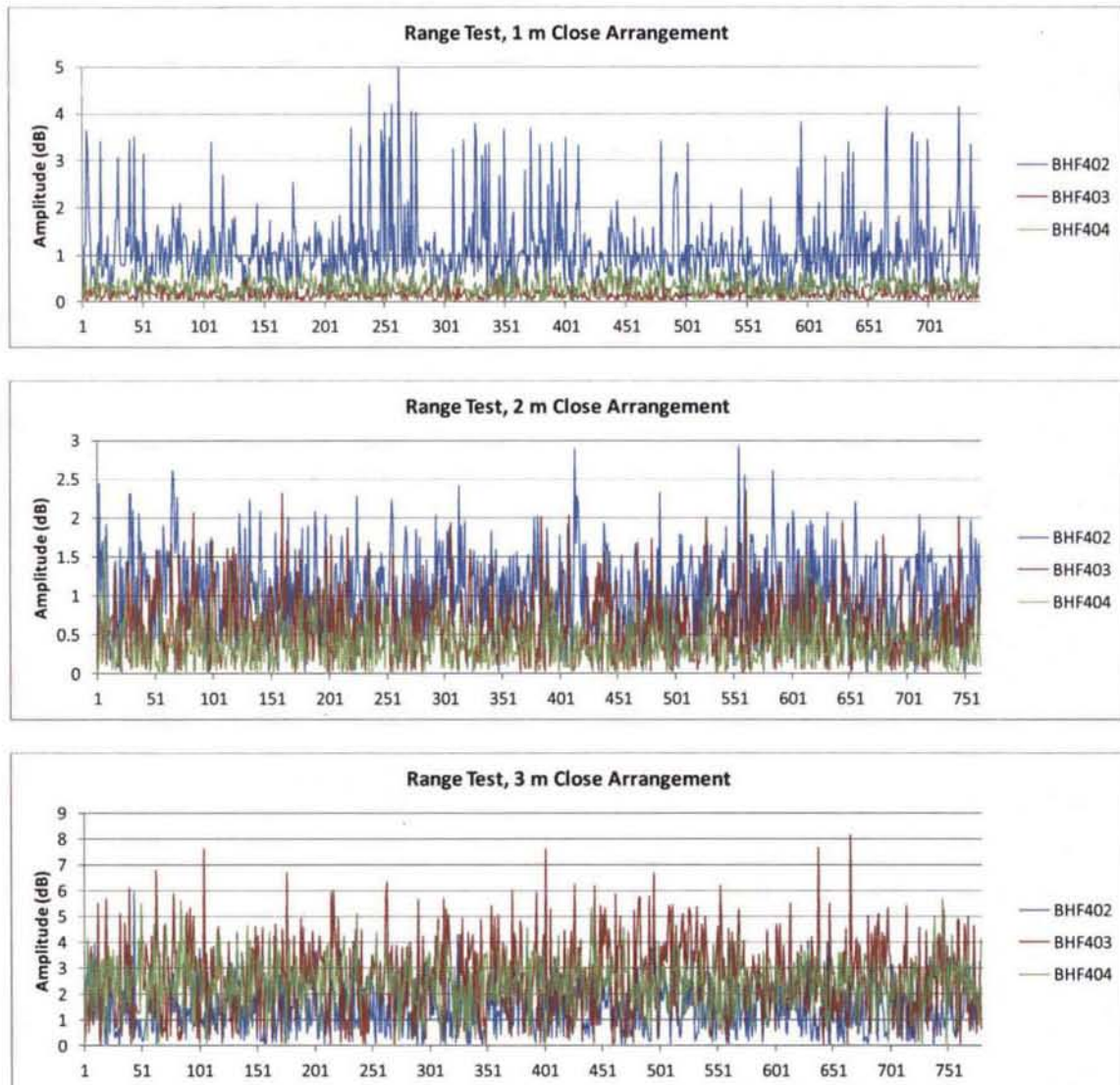
**Figure 38.    Range test results, amplitude**

### 2.5.3    Hydrogen Exposure Test

The hydrogen exposure test exposes the sensor alternately to breathing air and a low concentration of hydrogen in air. Concentrations of 2% and 3% hydrogen in air were tested; pre-mixed 1% hydrogen was not available at the time of testing. The actual commodities used are listed in Table 12 above. The test chamber is constructed from a piece of tubing approximately 6 inches (152.4 mm) long, with a nominal internal diameter of 51.6 mm. Thus the internal volume of the test chamber is approximately

$$\pi \times \left(\frac{51.6 \text{ mm}}{2}\right)^2 \times 152.4 \text{ mm} \times \left(\frac{1 \text{ L}}{10^6 \text{ mm}^3}\right) = 0.32 \text{ L},$$

plus the volume of associated tubing and fittings, and the flow path in the base of the test fixture. With a volume flow rate of 5 L/min, the test chamber volume will be changed out approximately 15 times per minute, or about once every 4 seconds, assuming uniform mixing. When testing multiple sensors simultaneously, to ensure each test fixture received the same flow rate, the fixtures were connected in a "daisy chain" configuration (see Figure 39), with the outlet of the first fixture connected to the inlet of the second fixture, and so forth. This was expected to introduce a small incremental delay in the sensors' response due to the additional volume which must be exchanged with each subsequent fixture, and this effect was observed in the results.

From Gas Supply
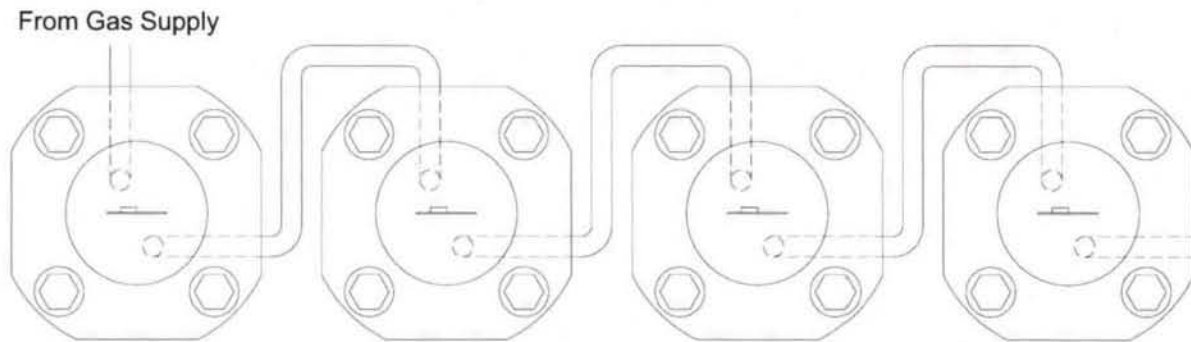


**Figure 39.    "Daisy chain" configuration**

Calibrated mass flow controllers were not available at the time the testing was conducted, thus uncalibrated mass flow controllers were compared on the bench to a laboratory standard flow measurement device, the CalTechnix molbox, with DH Instruments molbloc elements. This system uses a laminar flow element to generate a flow-dependent differential pressure; the pressure at the inlet and outlet of the element is measured by precision pressure transducers, and the temperature is also measured to compensate for temperature effects. The bench comparison was performed with compressed nitrogen gas, and the set points corresponding to the desired mass flow were recorded. The difference in flow controller performance (known as the gas correction factor or GCF) between nitrogen and air or hydrogen was not considered significant for the testing herein; however, the digital Sierra mass flow controllers were reconfigured for air after the bench comparison, since this feature is integral to the controller.

The test schematic is shown in Figure 40, and images of the actual setup are shown in Figure 41. Cylinders of breathing air and mixed hydrogen gas are fed to a three-way valve using standard cylinder regulators. The output of the three-way valve supplies a mass flow controller set for a target flow rate of 5 SLPM. By switching the three-way valve, the gas flow can be alternated between breathing air and mixed hydrogen gas fairly quickly. The test profile (for 2% gas) and results are shown in Figure 42. The time scales are shown approximately aligned; the hydrogen sensor software does not record a timestamp.
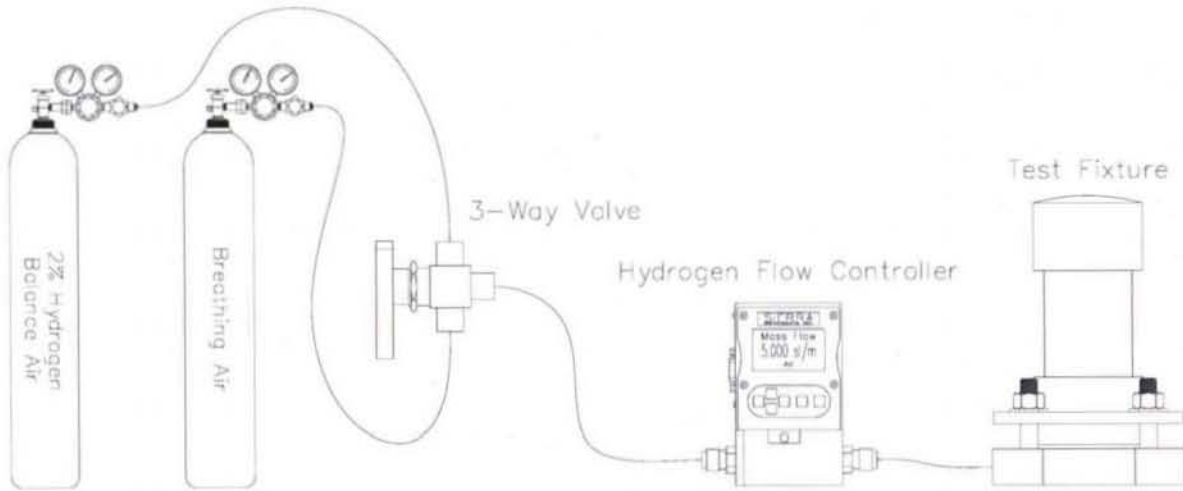
Figure 40.     Hydrogen exposure test setup schematic
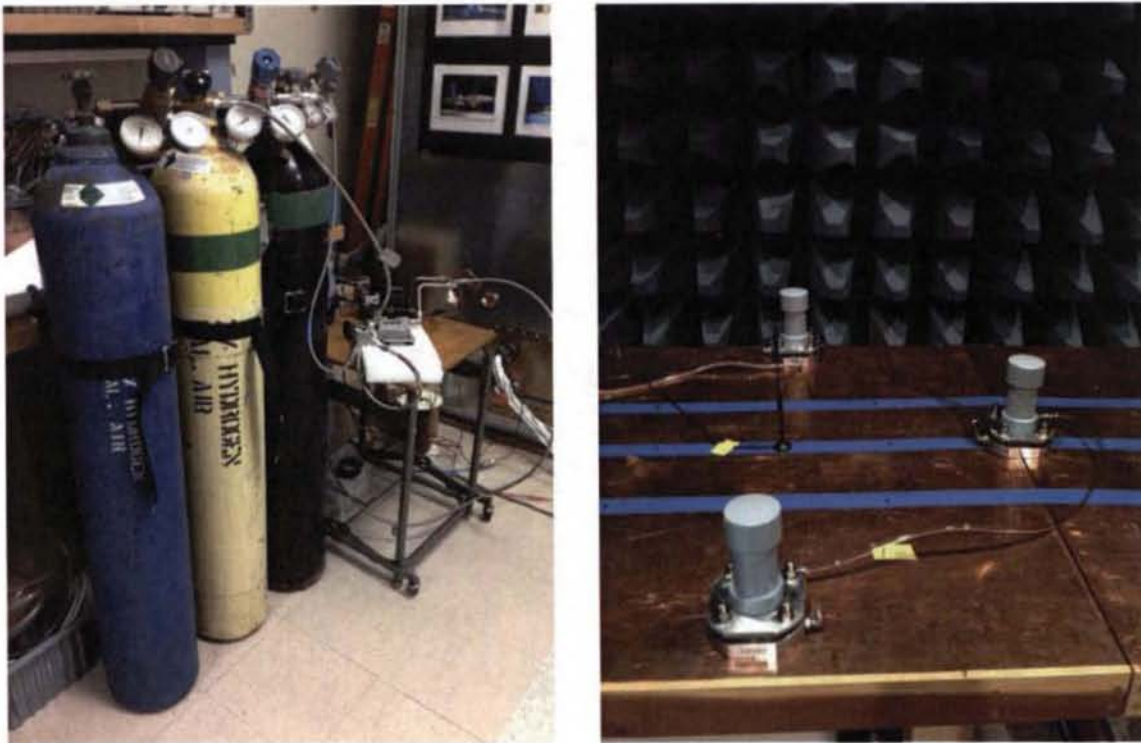


Figure 41.     Hydrogen exposure test setup overview; 90° arrangement shown
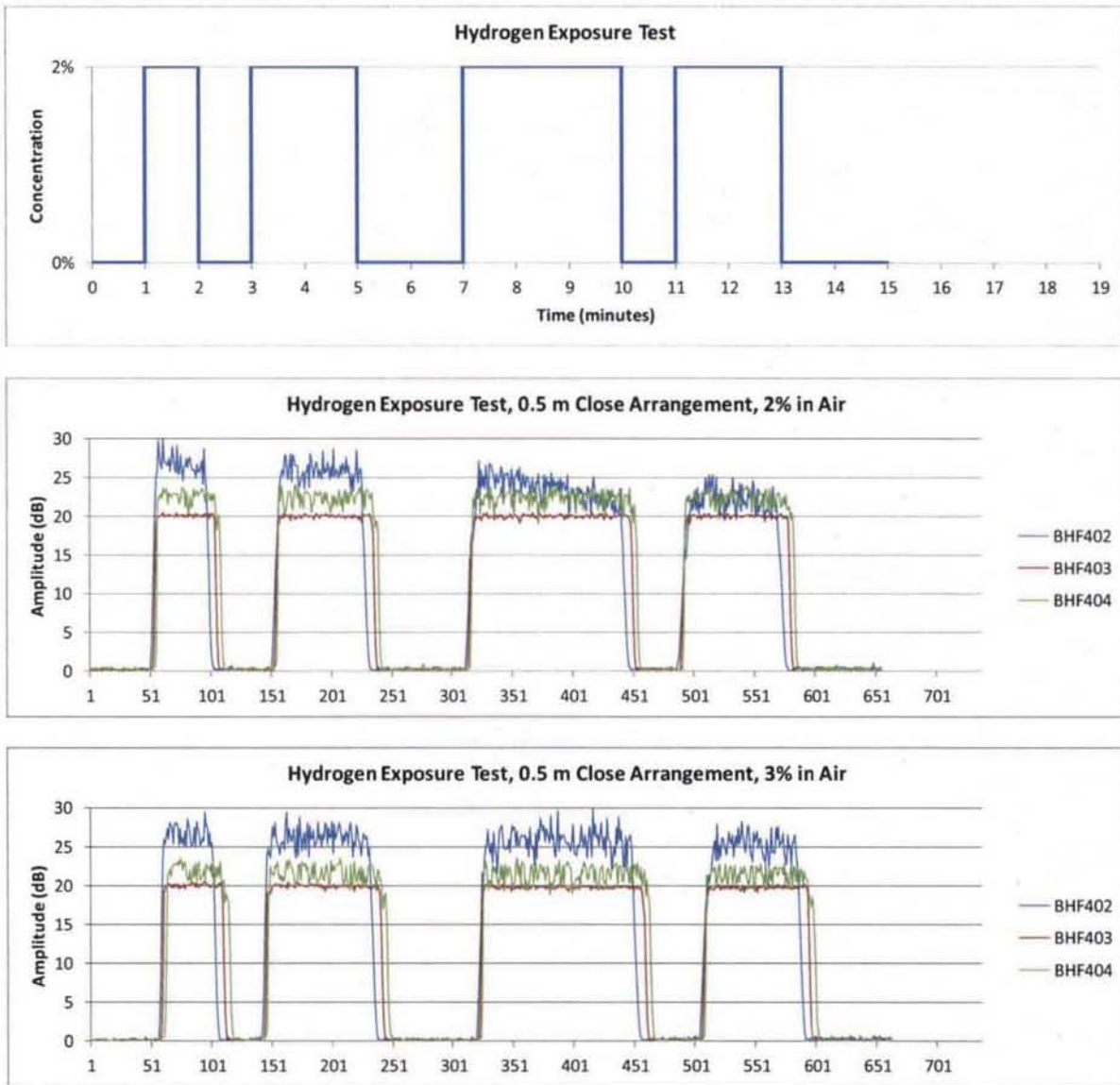
**Figure 42.    Hydrogen exposure test, input profile and results**

The hydrogen sensors track the input profile well. The expected lag due to the daisy-chain configuration is most visible when the gas is switched off; sensor BHF402 was first in the flow path, and sensor BHF404 was last. Also visible in the 2% hydrogen results is some slope in sensor BHF402; the reason for this is not known, and it was observed in some of the other test results. The similar amplitude between exposure to 2% and 3% hydrogen indicates that sensors BHF403 and BHF404 were saturated with exposure to 2%; sensor BHF402 may have been saturated or nearly so.

### 2.5.4 Hydrogen Concentration Test

The hydrogen concentration test exposes the sensor to varying concentrations of hydrogen by mixing breathing air with pre-mixed 2% hydrogen in air. The mix ratio is adjusted by using two mass flow controllers with their outputs connected in a tee fitting, as shown in Figure 43. The total flow rate is maintained approximately constant, and the flow controller set points are adjusted at the same time.
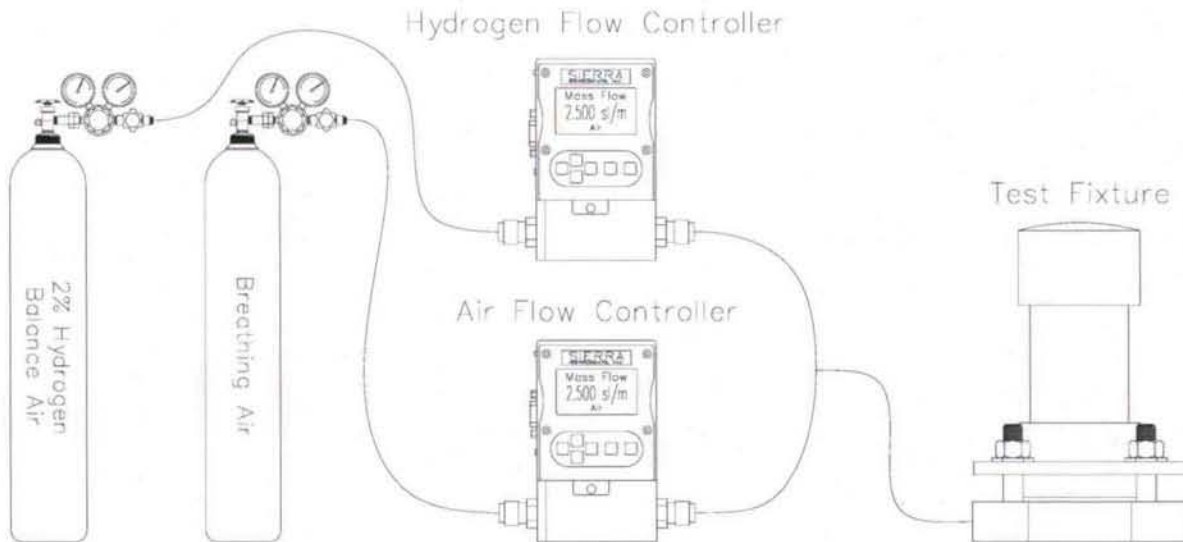


**Figure 43.** **Hydrogen concentration test setup**

The initial test was performed using a total mass flow rate of 8 SLPM, with the individual flow rates adjusted in steps of 0.8 SLPM to produce concentrations from 0.0% to 2.0% hydrogen in 0.2% steps. The higher flow rate (versus the exposure test) was due to the lower flow limit of the uncalibrated flow controllers. Sierra S/N 106457 was used for the 2% hydrogen, and Sierra S/N 106456 was used for the breathing air. The input concentration profile and the results of this initial test are shown in Figure 44; the time scales are approximately aligned. Saturation is observed for sensor BHF404 at 0.4% hydrogen and BHF403 at 0.6%; it is not clear whether sensor BHF402 saturates. Note also that hysteresis is observed in the data; the sensor performance with decreasing hydrogen concentration is different than the performance with increasing concentration.
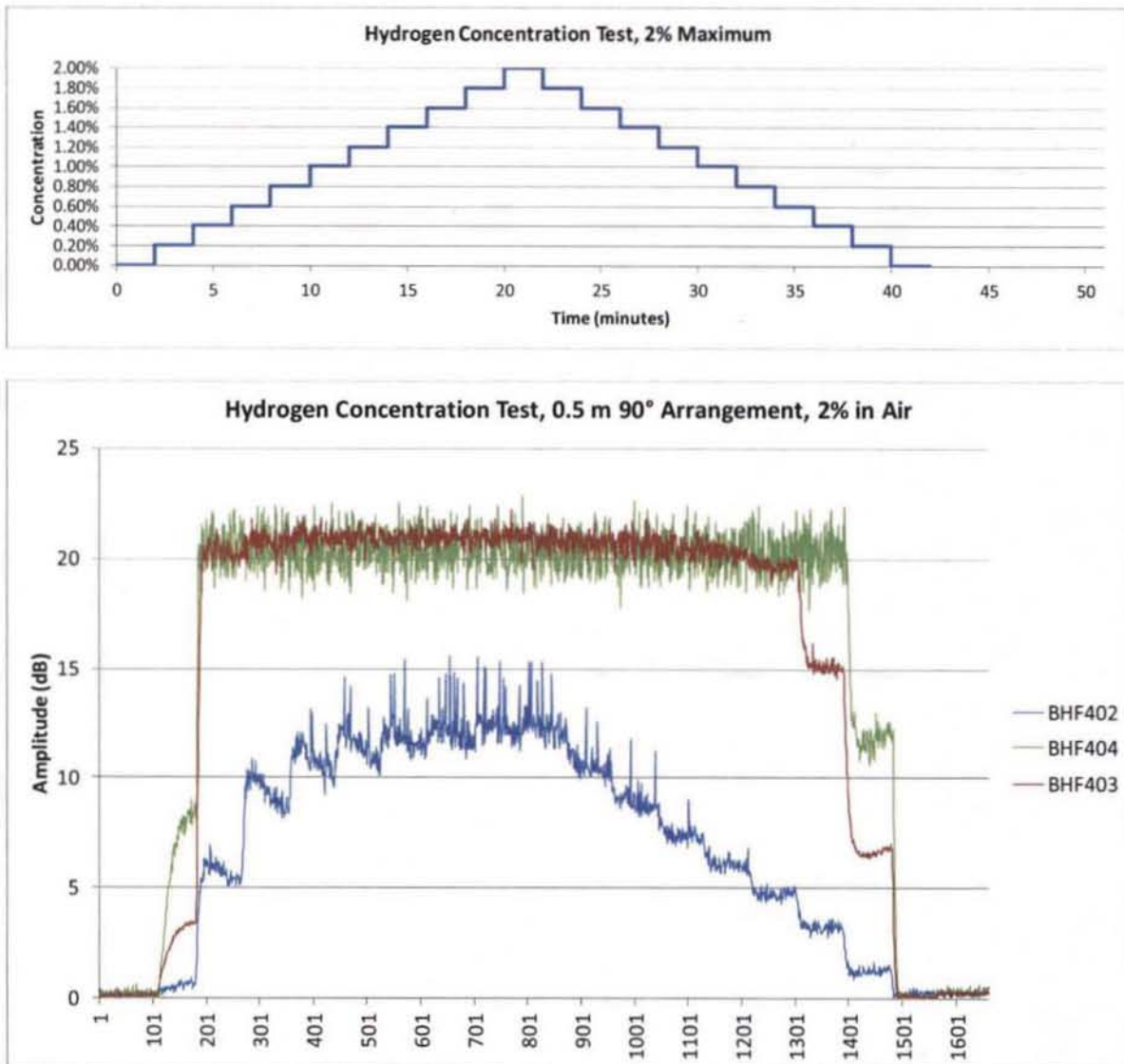
**Figure 44.     Hydrogen concentration test, input profile and results**

Because sensors BHF403 and BHF404 saturated so quickly, a second test was performed to assess the performance of the sensors at much lower hydrogen concentrations. Because of the limitations of using the 10 SLPM mass flow controllers at very low flow rates, an MKS M100B mass flow controller with a full scale of 1 SLPM was used to supply the 2% hydrogen and the total mass flow rate was increased to 9 SLPM to optimize the use of the MKS flow controller's range. Sierra S/N 106456 was again used for the breathing air supply. Since the M100B is an analog controller, a Yokogawa 7651 was used to supply the set point input, and a Fluke 8840A displayed the flow controller's measured output. The flow rate for each controller was adjusted in 0.09 SLPM increments to produce concentrations from 0.10% to 0.20% hydrogen in 0.02%

steps. The choice of 0.10% minimum was based on a previous test run, not shown here. The final step of the input profile was 0.12% rather than 0.10% due to a crash of the Sierra flow controller's display module. The input concentration profile and the results of this second test are shown in Figure 45; the time scales are approximately aligned.
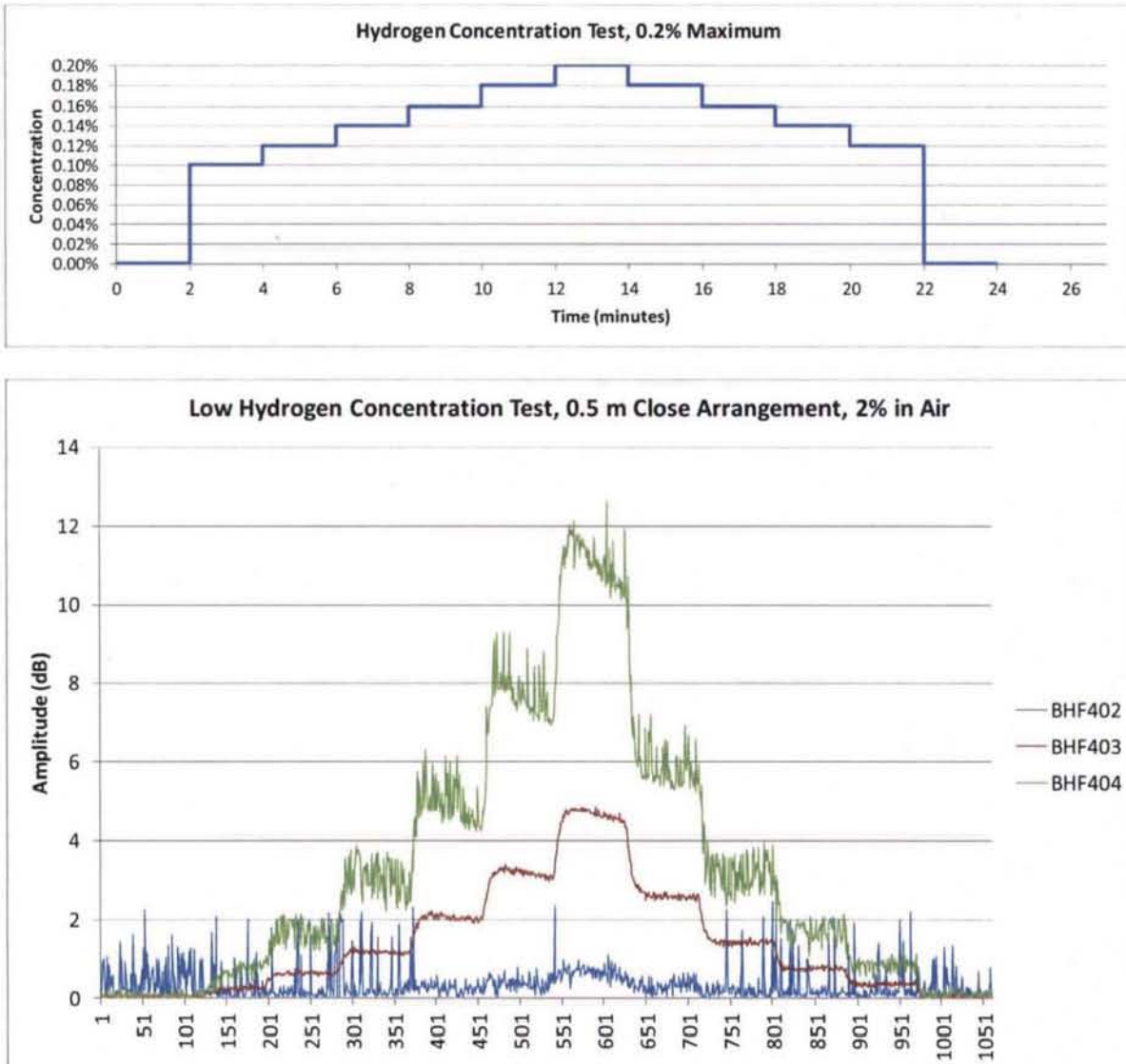


**Figure 45.    Low hydrogen concentration test, input profile and results**

## 2.5.5    Additional Testing

The testing in this section was not documented with the same level of detail as the testing above, as it was intended as an initial evaluation of some of the other factors which may influence sensor performance. The first factor considered was helium. Existing hydrogen sensor

41

technologies used at KSC have, at times, exhibited poor performance when exposed to helium. Two tests were performed using a mixture of nominally 50% helium and 50% breathing air; the actual concentration (see Table 12) was 62.6% helium and 37.4% breathing air. A gas correction factor of 1.191 for 50% helium and 50% breathing air was calculated from Sierra's user manual and published data for breathing air composition. The first test used the MKS flow controller to supply the helium mixture, and Sierra S/N 106456 to supply breathing air, with a total flow rate of 9 SLPM. With a concentration mixed to 6.26% helium (based on the actual concentration), no response from the sensor was observed, as shown in Figure 46; the input concentration profile was not recorded. The slope observed in the data is similar to that observed in the baseline test.
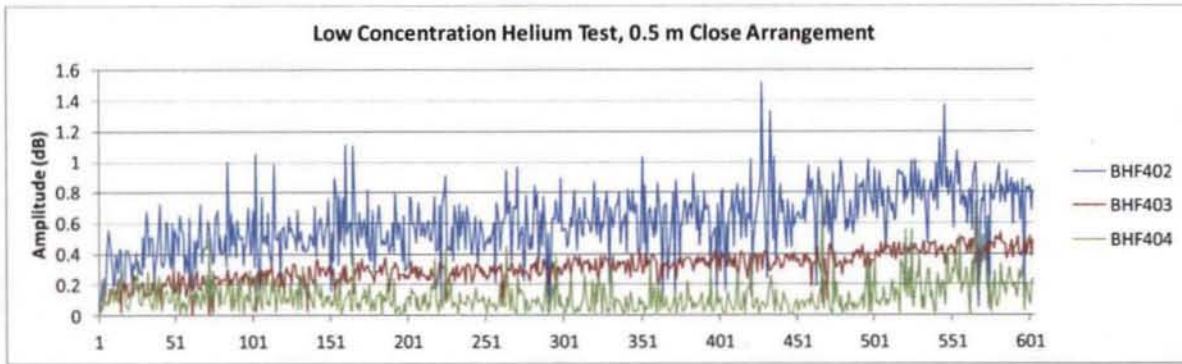


**Figure 46.**     **Low helium concentration test results**

In the second test, the helium mixture was switched to the Sierra flow controller, and 2% hydrogen in air was supplied using the MKS controller, with a total flow rate of 9 SLPM. A few test concentrations were applied; these are annotated in Figure 47. The maximum hydrogen concentration of 0.20% corresponds to a helium concentration of approximately 56.3%; at 0.00% hydrogen, the helium concentration is that of the mixed helium cylinder, 62.6%. It was observed that with these high concentrations of helium, the hydrogen sensitivity seemed to be significantly higher; note that both sensors BHF403 and BHF404 come close to their saturation values with 0.2% hydrogen; compare this to the amplitude values in Figure 45.
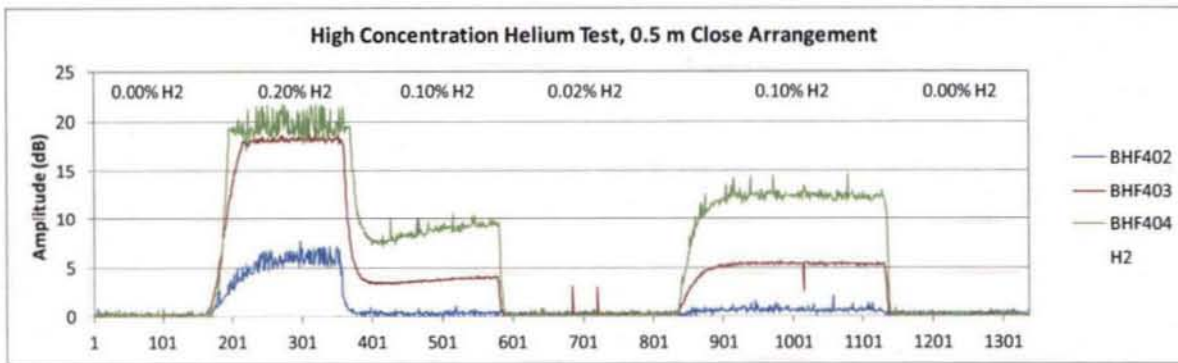


**Figure 47.**     **High helium concentration test results**

Since it was not expected that the thin film would respond to helium, a hypothesis was developed that the increased sensitivity might be due to the lower oxygen concentration. To test this hypothesis, the sensors were exposed to 2% hydrogen in nitrogen, which was supplied using the Sierra S/N 106456 controller. After the sensors saturated, the flow was continued to ensure the oxygen in the test enclosures was displaced. The flow was then terminated, and the amplitude data was monitored. It was noted that the sensors remained saturated even after the termination of flow and the disconnection of the supply line, despite the fact that the small amount of hydrogen in each test enclosure was expected to stratify fairly quickly at the top of the enclosure. The supply line was then reconnected, and the controller was switched to breathing air at a low flow rate. The exposure to breathing air slowly returned the sensors to their background noise levels. To confirm that the effect was due to the lack of oxygen rather than the lack of gas flow, the exposure test could be performed with test gases of nitrogen and 2% hydrogen in nitrogen instead of breathing air and 2% hydrogen in air; if the lack of oxygen does not allow the sensors to recover, then the sensors should remain saturated after the first exposure to hydrogen.
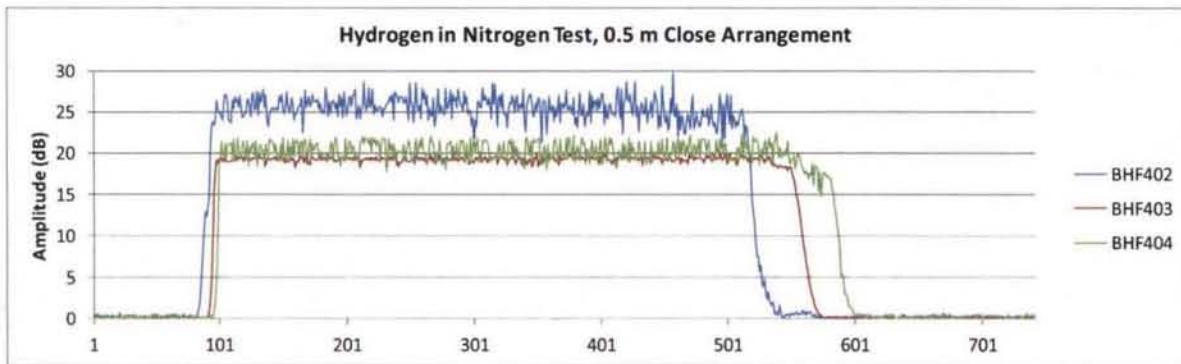


**Figure 48.    Hydrogen in nitrogen test results**

## 2.6    Other Support

Also supported on this task order was the receiving and demonstration of the ASR&D Corporation wireless humidity sensor system, delivered to KSC under STTR Phase II contract NNX09CB77C, and associated NASA property management actions. Characterization testing of this system is not currently within the scope of this task order.

## 3.    CONCLUSIONS AND RECOMMENDATIONS

## 3.1    Summary of Results

RF characterization of the Mnemonics-UCF SAW sensor system shows significant broadcast power outside the ISM band, both at the fundamental frequency (which was expected) and in the harmonics, which are observable above the background noise out to the fifth harmonic. The second harmonic is only 20 dB down from the fundamental. The low repetition rate of the system makes RF analysis challenging; data capture was improved through the creation of a MATLAB script to increase the query repetition rate. The use of a high-speed oscilloscope

makes single-shot characterization possible for the fundamental frequency band and the time-domain characteristics of the interrogator pulse. Near-field probe test data has been captured, but has not yet been analyzed.

When capturing data as a temperature measurement system, the relative orientations and spacing of the antenna and sensor strongly affect the stability of the measurement and the ability to capture useable data. The operating software currently has no means to determine when valid sensor data is present. Relative differences were observed in the performance of the four supplied temperature sensors. Ground plane effects may also strongly affect the performance of the sensors in some orientations. Free-space range was tested for a single sensor and found to be less than 5 m for the default integration time of the system. Stable, low-noise operation was observed with a short distance (0.5 m) between the sensor and antenna. When considered on an aggregate basis, the collected data shows a strong, fairly consistent trend in the relationship between the standard deviation of the data, taken to be the noise level, and the software's calculated correlation peak, taken to be the signal level. Initial temperature testing shows good correlation between the sensor data and measurements taken with a calibrated thermocouple readout.

When capturing data as a hydrogen measurement system, the sensors respond quickly to changes in ambient hydrogen concentration, down to levels as low as 0.1% in air. The three sensors tested had significant differences in their sensitivity to hydrogen. Sensor noise levels increase with increasing distance, though response to hydrogen was not tested at distances other than 0.5 m. Also, some hysteresis and slope was observed in the data; it is not known whether these effects are due to the sensor response or due to factors in the test setup, such as stratification of the mixed gas in the cylinders.

## 3.2    Conclusions

Given the RF output levels at frequencies allocated to other devices, it is not anticipated that the sensor system will be approved for use at KSC outside the EMI test chamber. Possible mitigations could include an ISM filter on the output of the interrogator, though this may significantly reduce the performance of the system by truncating the RF spectrum used by the sensors.

As a system, temperature can be measured with relatively small amounts of noise when the interrogator antenna and sensor are sufficiently close together, and in favorable relative orientations. The correlation peak value calculated by the software could be used to estimate the confidence interval of a given measurement. System accuracy is yet to be determined, and will require testing with more sensors over wider ranges of temperature, but initial results show good tracking of the actual temperature profile. Hydrogen can be sensed at fairly low concentrations, well below the 4% lower flammability limit for hydrogen in air. Again, system accuracy is yet to be determined, and each sensor shows different sensitivity.

## 3.3     Recommendations

Future testing should include wider ranges of temperature to characterize accuracy performance for the temperature sensors. Temperature measurement performance should also be tested with multiple sensors. The trend between sensor noise and correlation peak should be improved by the addition of more data, to determine whether this would be a reasonable predictor of the accuracy of sensor measurements. The effects of integration time on sensor noise and accuracy should be examined. For the hydrogen sensors, concentration tests should be repeated to determine whether the sensors can be reliably calibrated, which would be necessary for determining accuracy. Hydrogen sensitivity could be tested with more confidence at low levels by procuring a mixed gas cylinder with a lower concentration of hydrogen in air, such as 0.4%; this could be used for both the exposure test and the concentration test, where it could be mixed to even lower concentrations. The hydrogen measurement software would also benefit from the addition of a timestamp to the recorded data files, which would allow the temporal correlation of the input profile and the measured data. The signals observed in the quiet EMI chamber should be identified, which may be possible by terminating the input of the spectrum analyzer and observing whether a nearby GSM cell phone may be detected.

## APPENDIX A.    NEAR-FIELD PROBE TEST RESULTS

Following is the data collected during near-field probe testing. Spectrum captures are given for each of the internal components indicated in the images.
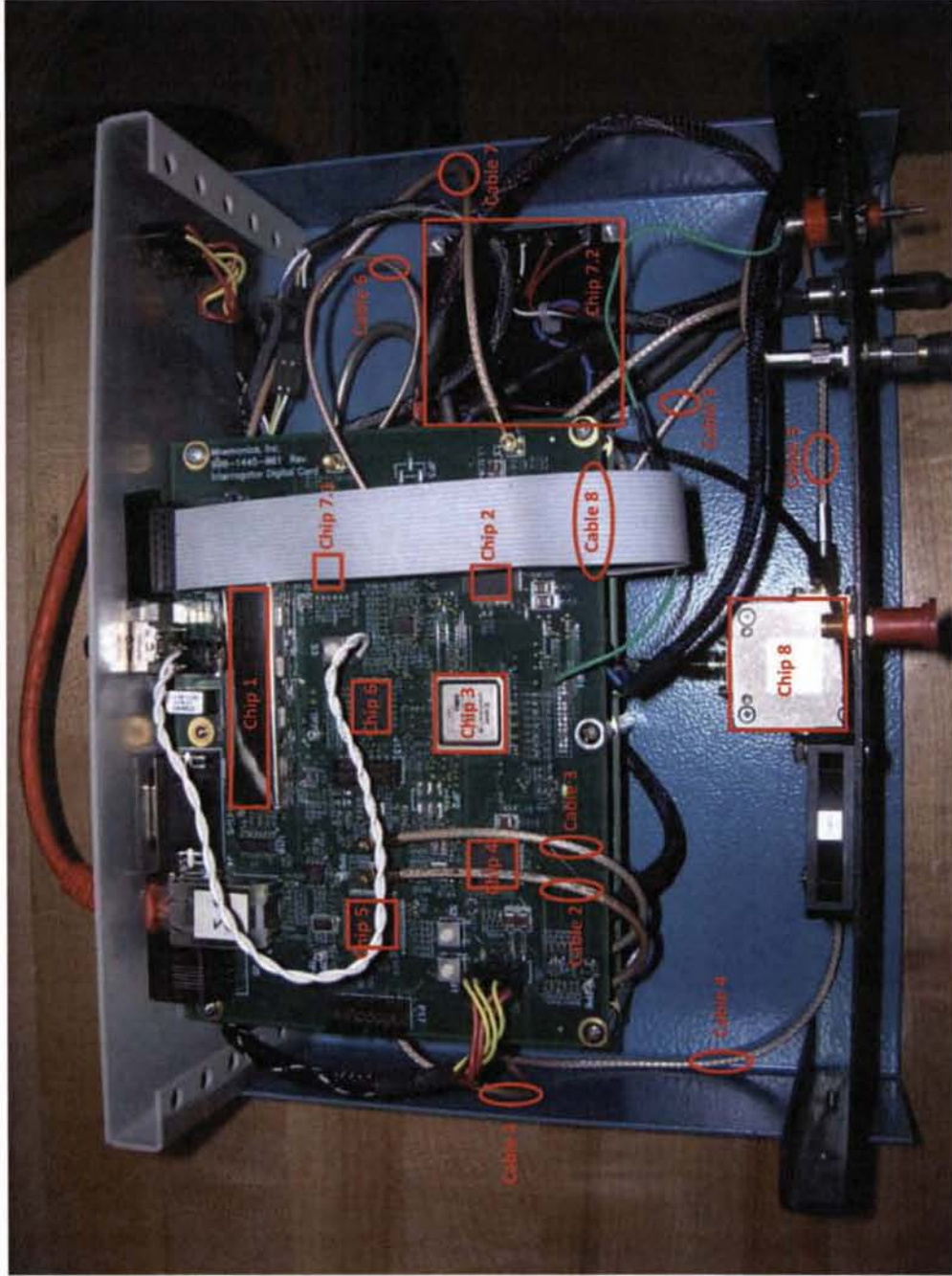
Upper board and cabling

47

Lower board

**Test setup; pre-amplifier is shown at the top; near-field probe and interrogator are at lower right**

**Chip designations (where available); for cables, see image**

| Chip 1 | ? |
| --- | --- |
| Chip 2 | U18 |
| Chip 3 | U14? |
| Chip 4 | ? |
| Chip 5 | U13 |
| Chip 6 | U27 |
| Chip 7.1 | ? |
| Chip 7.2 | DC/DC Converter? |
| Chip 8 | RF Combiner? |
| Chip 9 | U12 |
| Chip 10 | U13 |
| Chip 11 | ? |
| Chip 12 | ? |
| Chip 13 | ? |
| Chip 14 | ? |
| Chip 15 | ? |

Equipment Used:
   Agilent E7405A Spectrum Analyzer
   Agilent 11940A Near-field Probe
   HP 8447F pre-amp
   09-09-407 60″ cable
   08-08-801 39.7″ cable

Equipment Settings:
   30 MHz – 1 GHz Span
   RBW 120 kHz, VBW 300 kHz
   AC Coupled
   Max Hold for 2.5 min
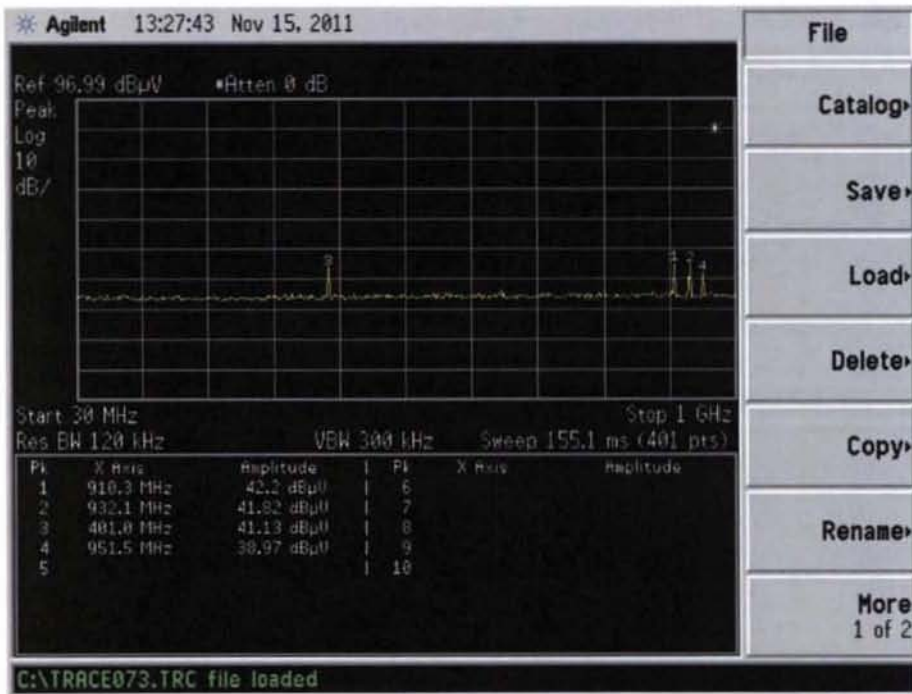
**Chip 1**
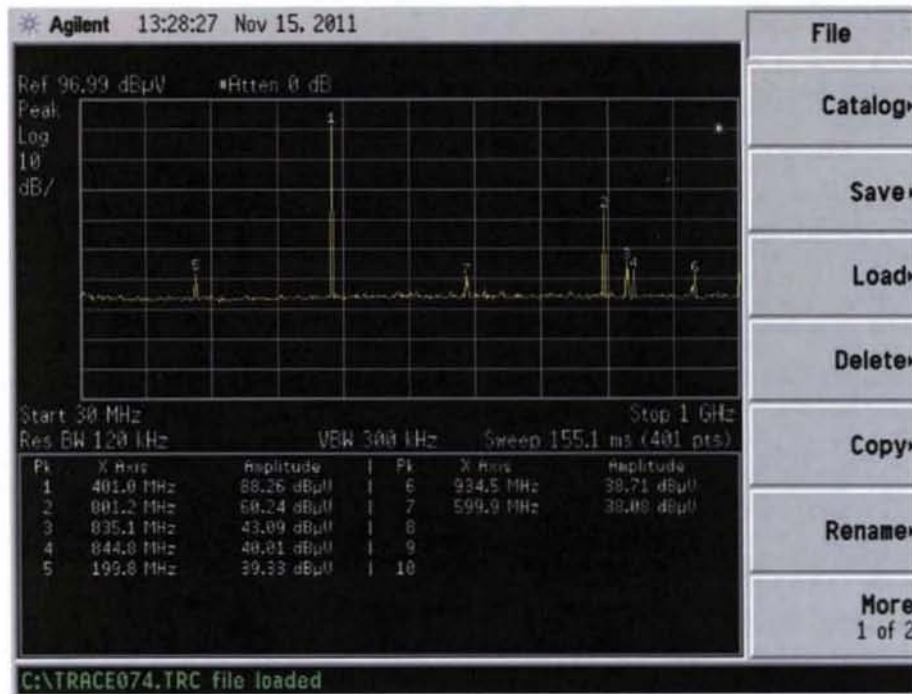


**Chip 2**
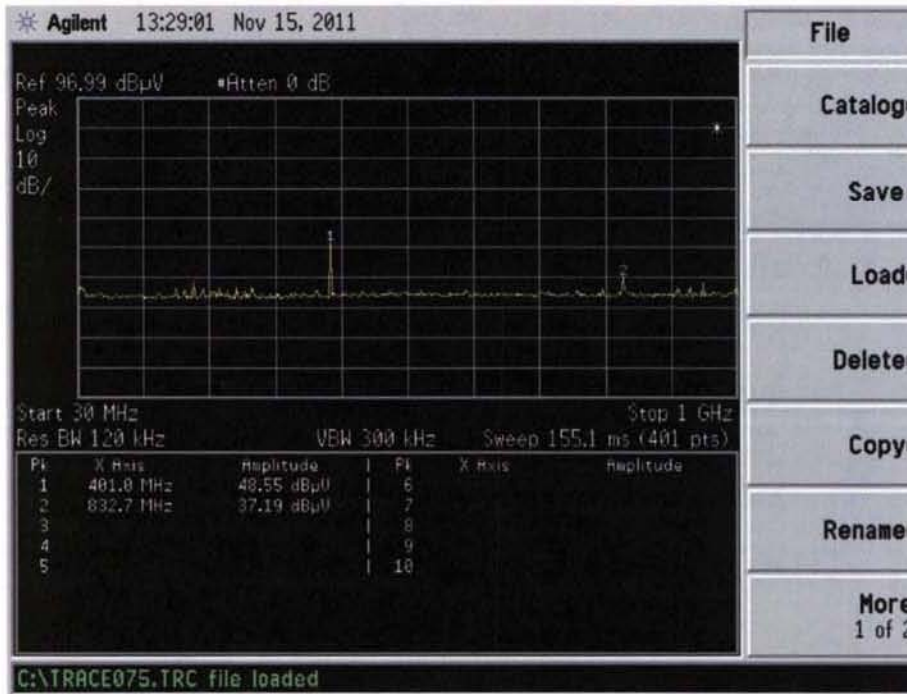
**Chip 3**
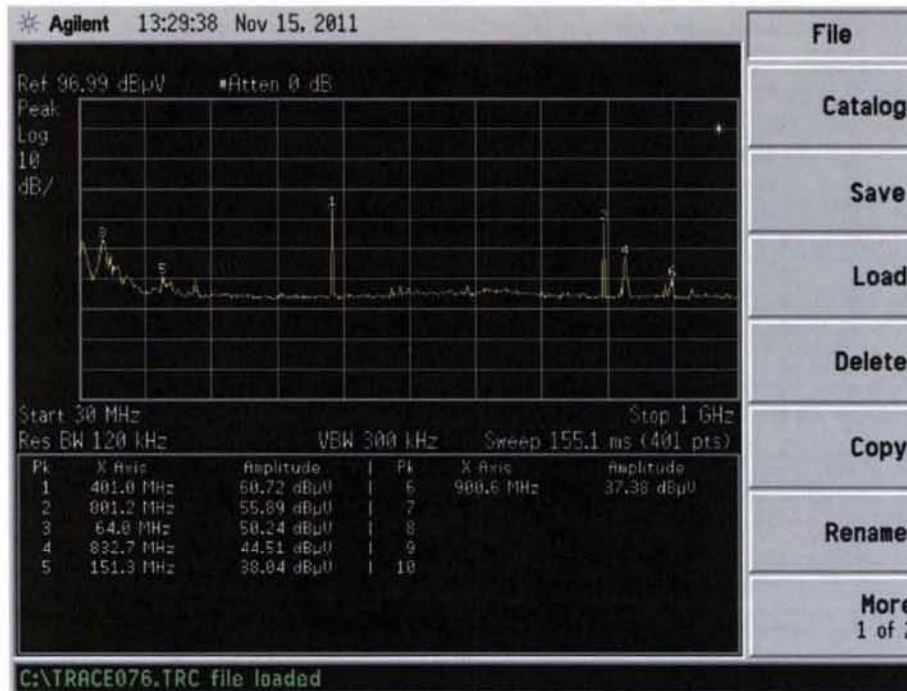


**Chip 4**
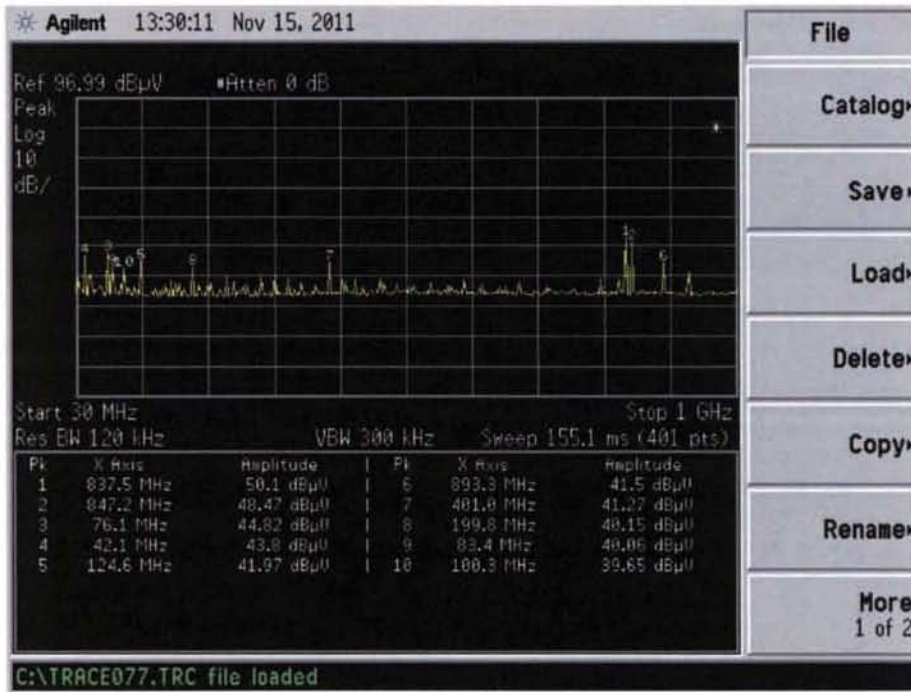
**Chip 5**
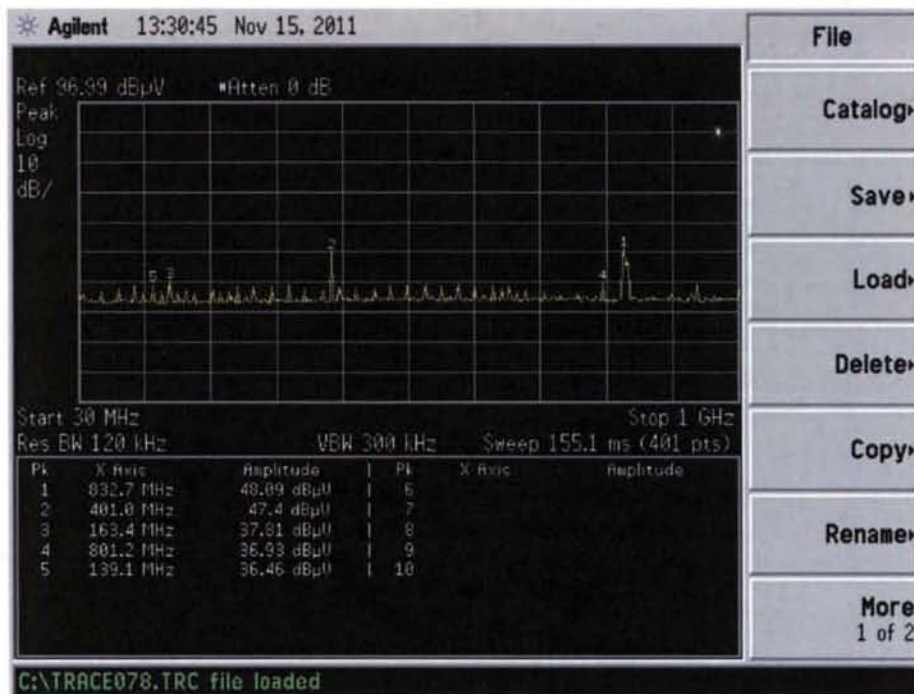


**Chip 6**
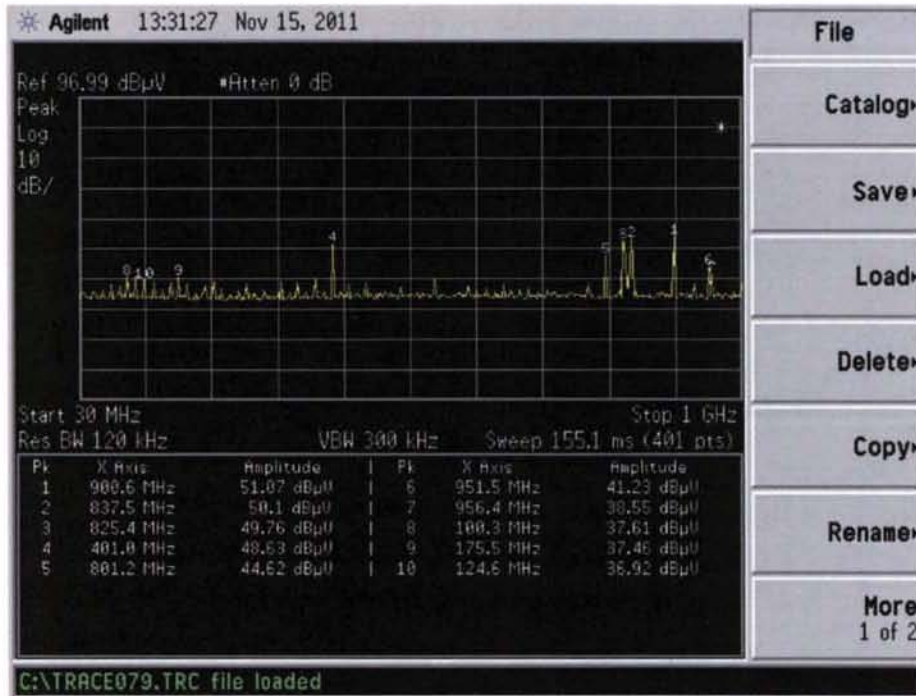
**Chip 7.1**



**Chip 7.2**
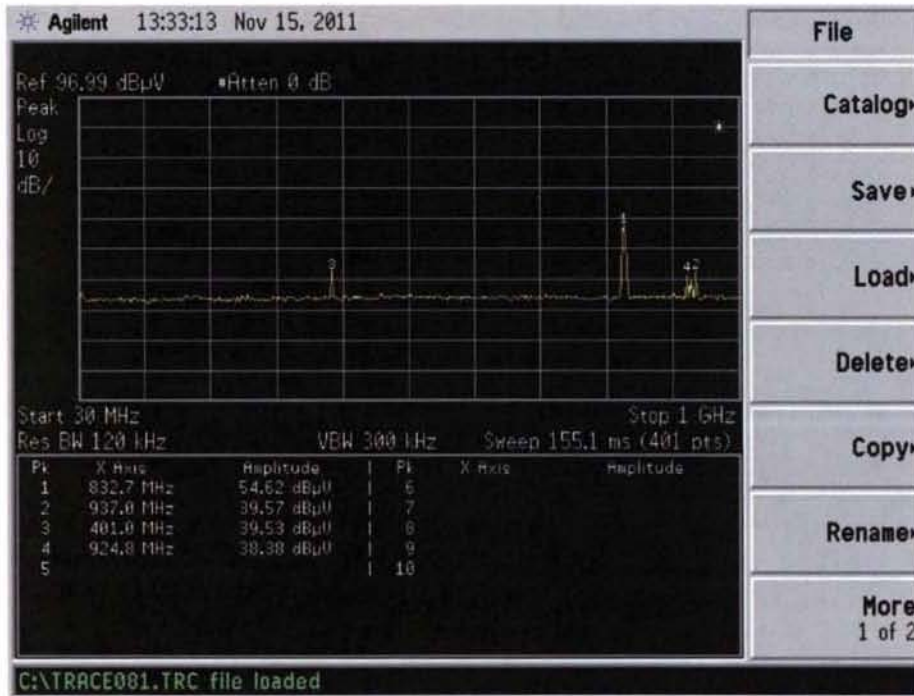
**Chip 8**
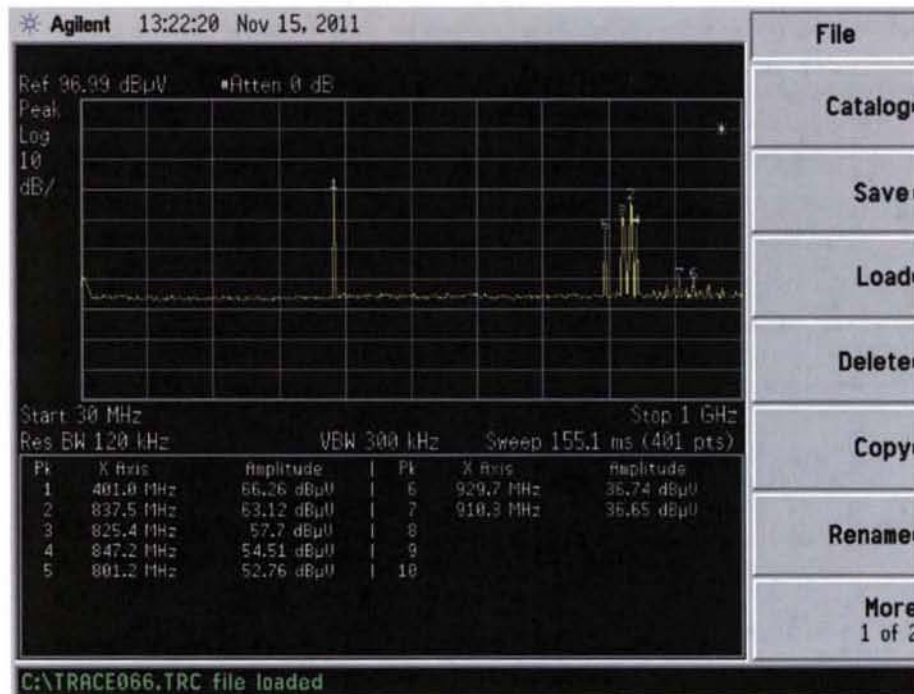


**Chip 9**
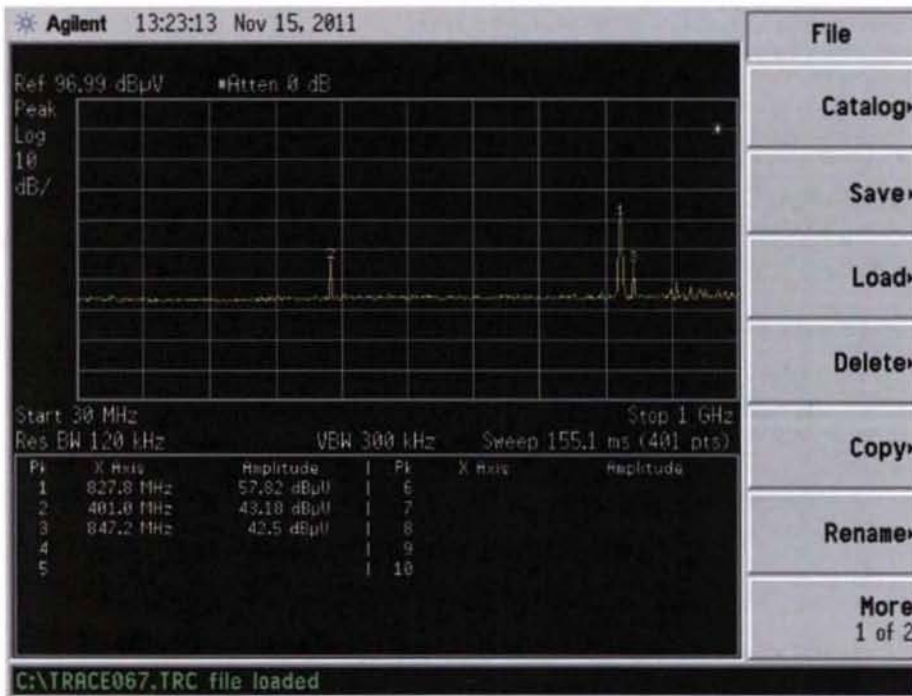
**Chip 10**
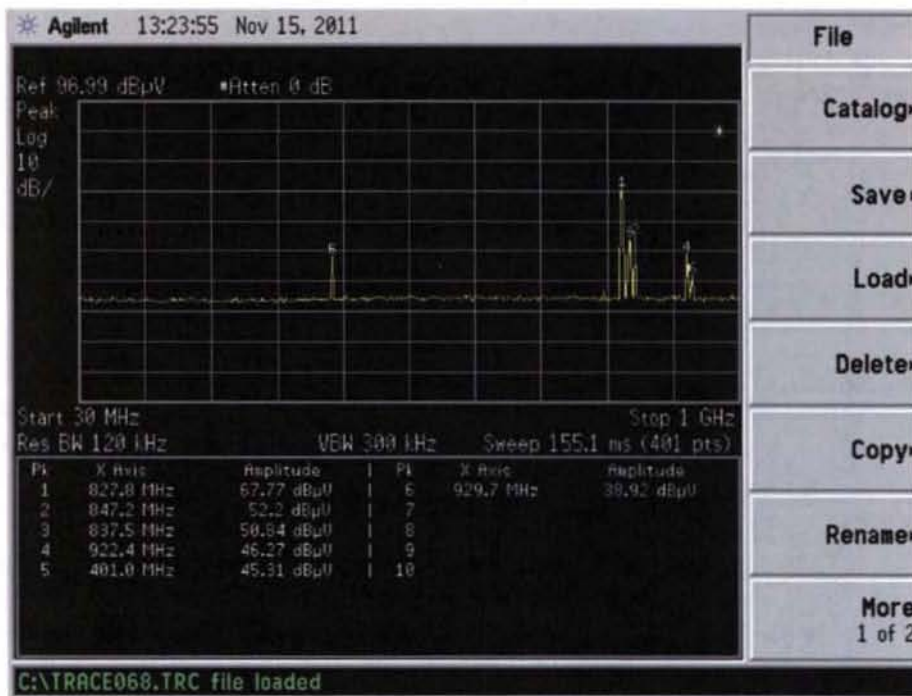


**Chip 11**
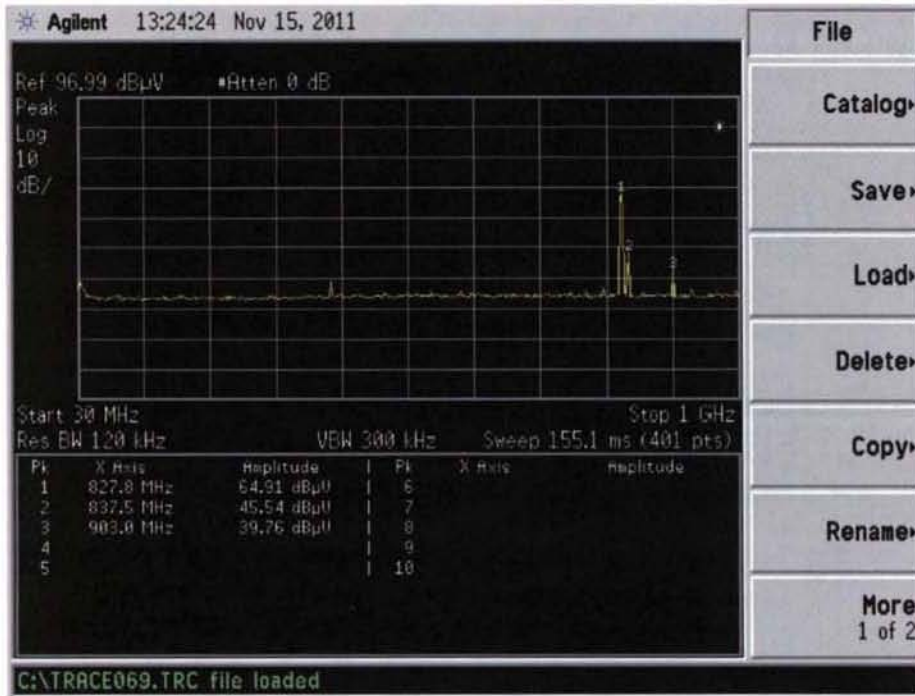
**Chip 12**
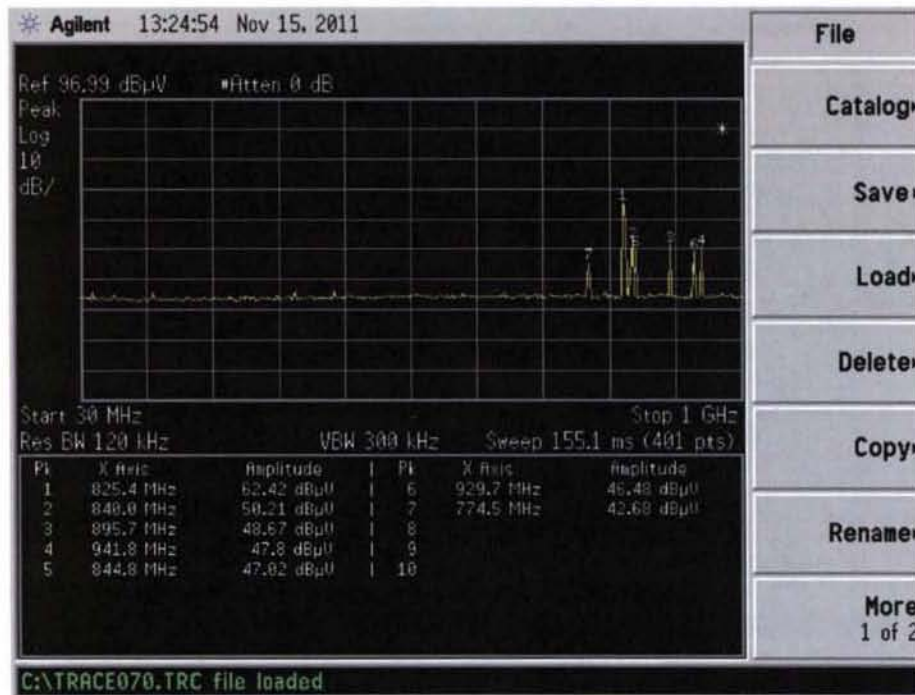


**Chip 13**
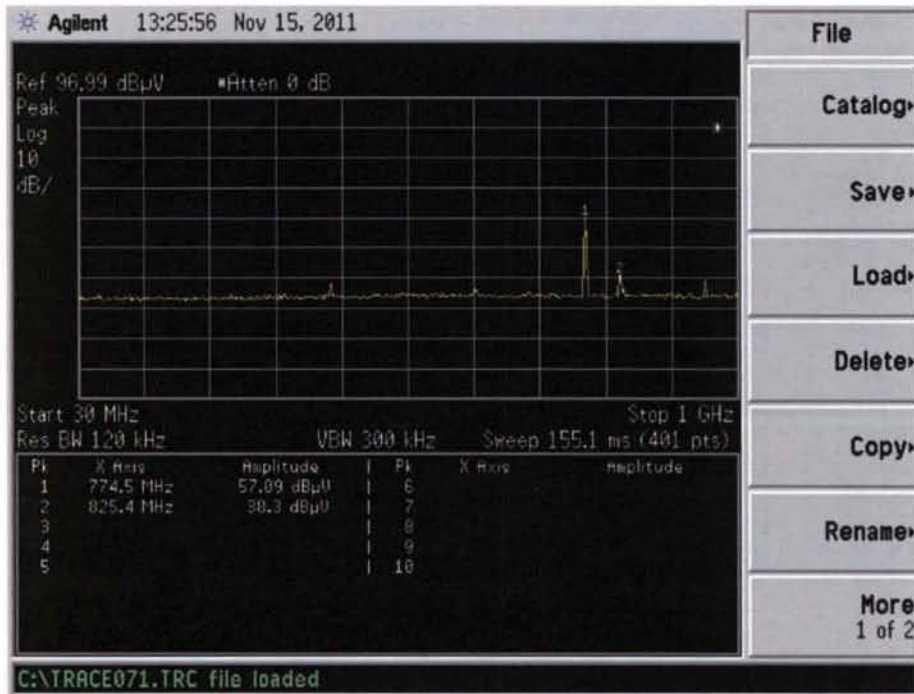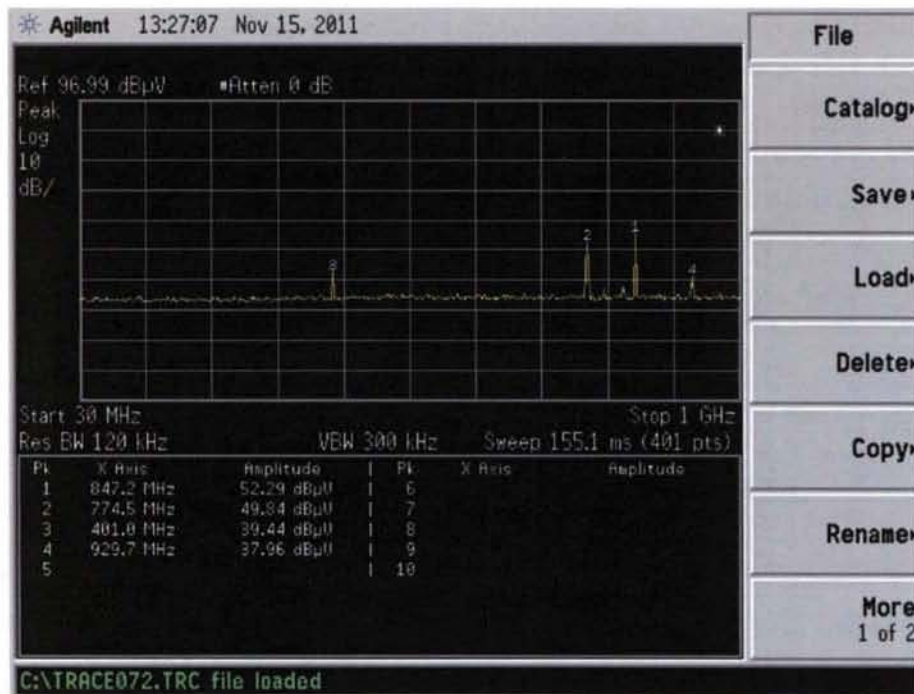
Chip 14



Chip 15

**Cable 1**
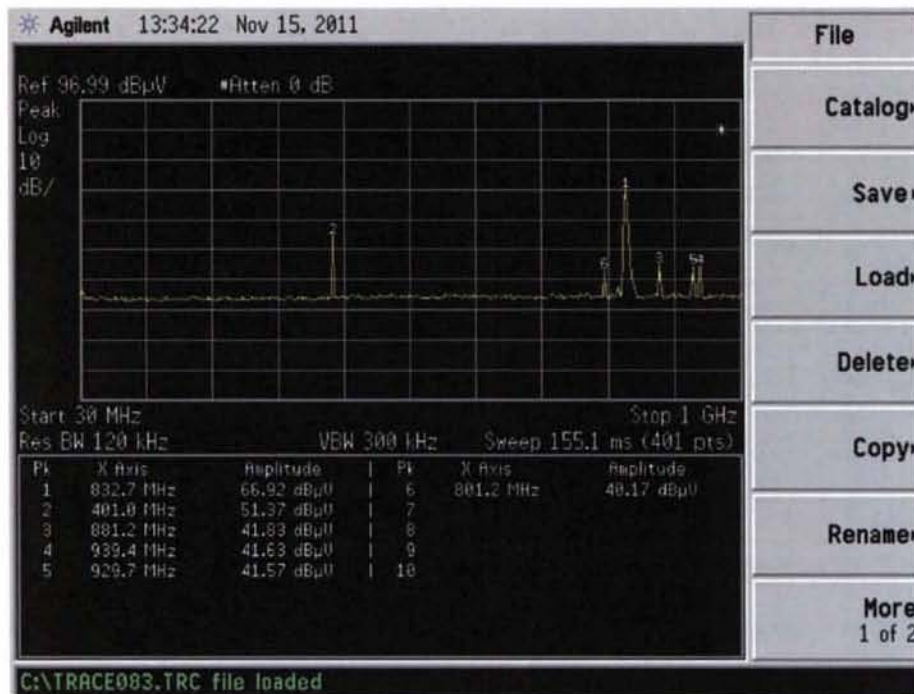


**Cables 2 & 3**
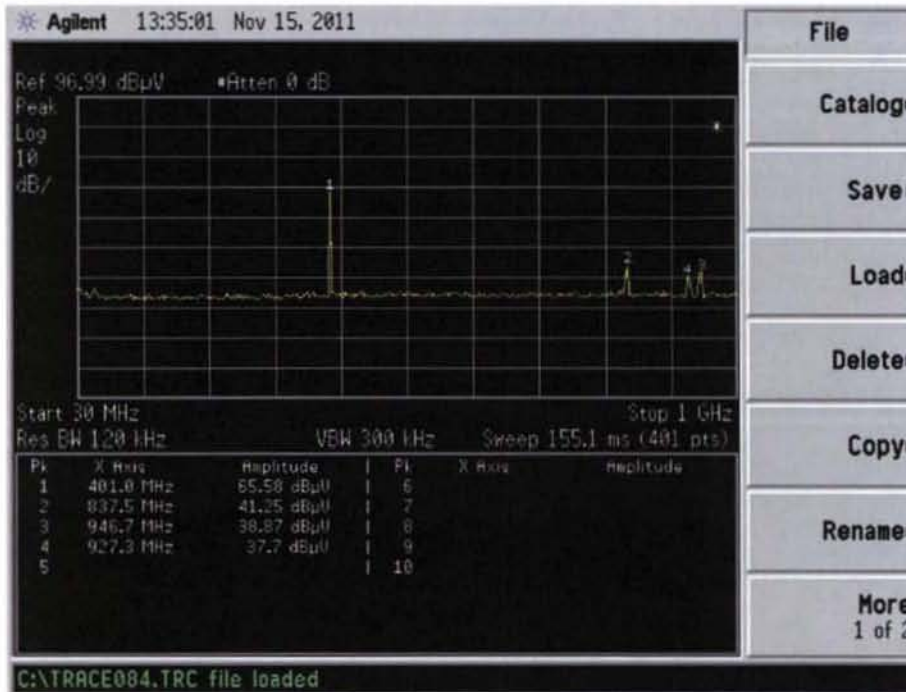
**Cable 4**
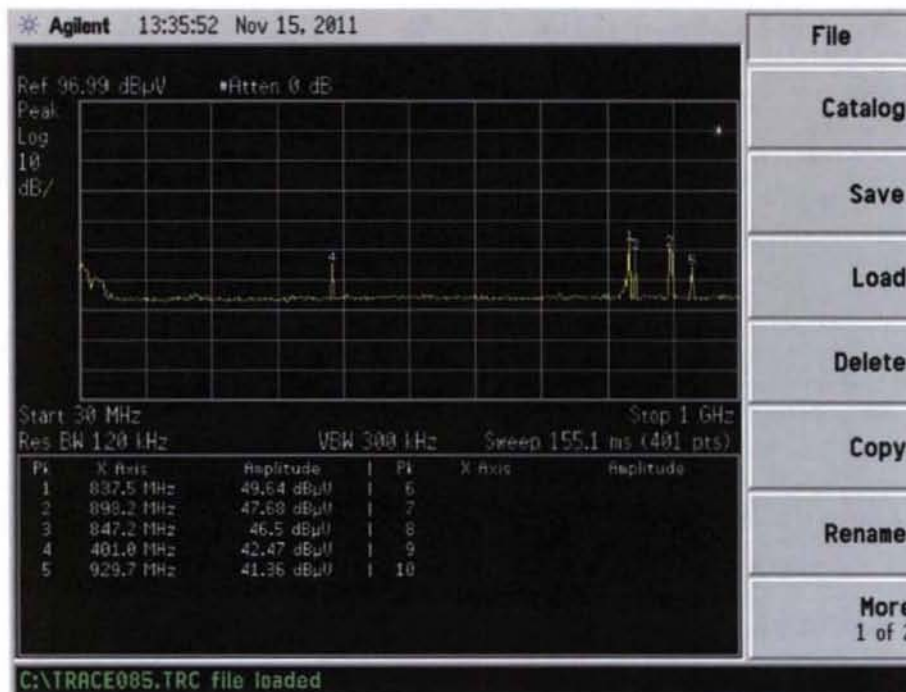


**Cable 5**
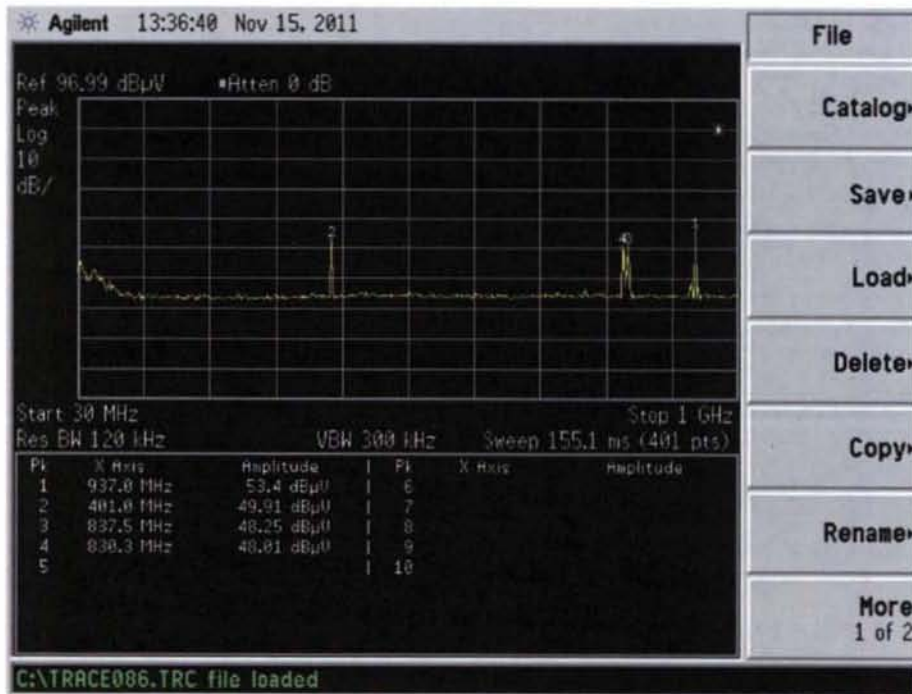
Cable 6



Cable 7

**Cable 8**



**Cable 9**

## APPENDIX B.    DATA SHEETS

Following is the data summary sheet from the temperature testing herein, representing 81 individual data files (over 42,000 points), which are stored separately.

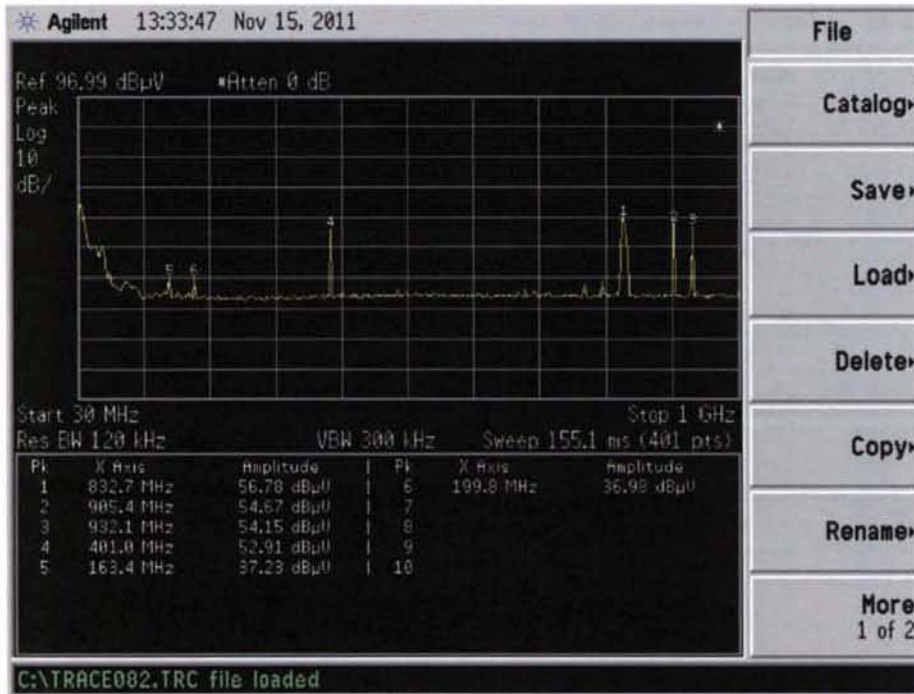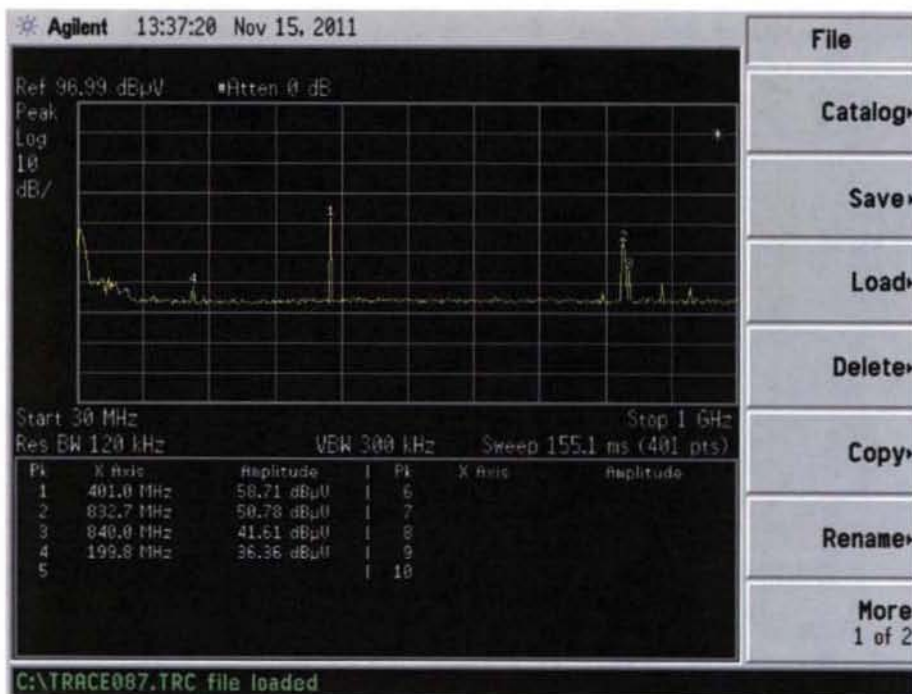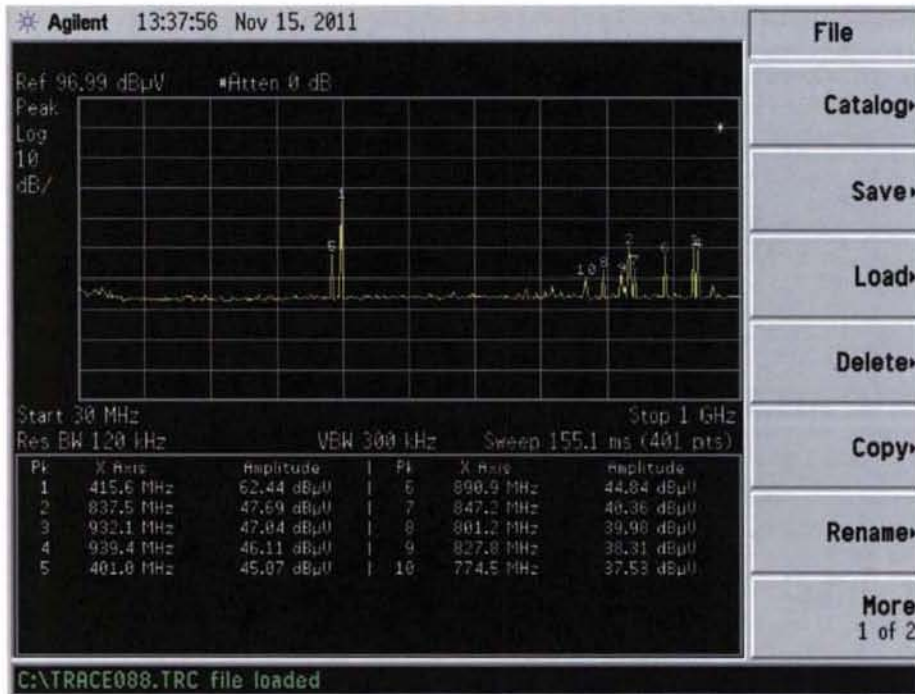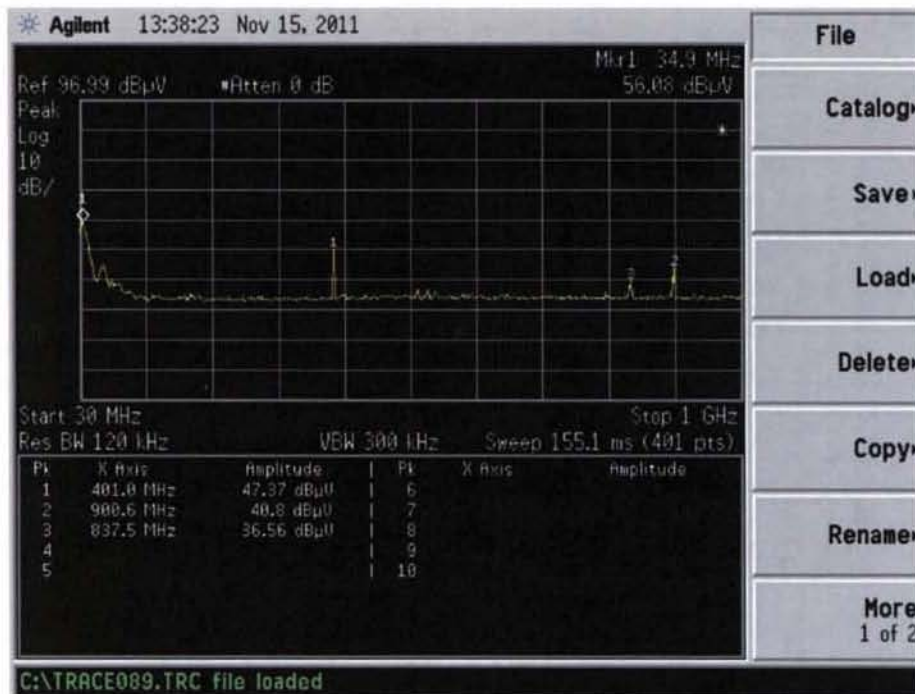| File | Sensor | Orientation | Distance (m) | Test | Notes | Temp Start (°C) | Temp Stop (°C) | Exhaust Fans | Location | Rows | Temperature Avg (°C) | Temperature Std Dev (°C) | Residual (21-pt median) Avg (°C) | Residual (21-pt median) Std Dev (°C) | Correlation Peak Avg (dB) | Correlation Peak Std Dev (dB) |
|---|---|---|---|---|---|---|---|---|---|---|---|---|---|---|---|---|
| SAW Data 2011-09-27 13.51.04.txt | NS401R | 1: Vertical | 0.25 | Range/stability | | | | TRUE | Table | 620 | 25.42472859 | 0.314165774 | -0.053031002 | 0.247837308 | | |
| SAW Data 2011-09-27 14.28.06.txt | NS401R | 2: Horizontal | 0.25 | Range/stability | | | | TRUE | Table | 605 | 19.99307119 | 21.19261864 | -2.824024834 | 21.12822363 | | |
| SAW Data 2011-09-27 15.15.38.txt | NS401R | 3: Rotated Vertical | 0.25 | Range/stability | | | | TRUE | Table | 582 | 25.64617384 | 0.251706388 | -0.061624785 | 0.226042116 | | |
| SAW Data 2011-09-27 15.51.03.txt | NS401R | 4: Rotated Horizontal | 0.25 | Range/stability | | | | TRUE | Table | 645 | 23.8308124 | 0.138747063 | -0.008562112 | 0.135548597 | | |
| SAW Data 2011-09-27 16.30.52.txt | NS401R | 1: Vertical | 0.5 | Range/stability | Added correlation peak in dll, but lost seconds. | | | TRUE | Table | 534 | 24.32026829 | 0.105359166 | -0.00258349 | 0.102123392 | 72.08325516 | 0.043669626 |
| SAW Data 2011-09-28 09.44.34.txt | NS401R | 1: Vertical | 0.5 | Range/stability | Repeat next day to verify correlation peak functionality. | | | TRUE | Table | 611 | 24.33182623 | 0.09410679 | -0.00377623 | 0.0876639893 | 72.09014098 | 0.030410921 |
| SAW Data 2011-09-28 10.57.17.txt | NS401R | 2: Horizontal | 0.5 | Range/stability | | | | TRUE | Table | 1063 | 21.48384275 | 14.32825181 | -0.752379473 | 14.23176665 | 38.18148305 | 1.245861325 |
| SAW Data 2011-09-28 12.09.00.txt | NS401R | 3: Rotated Vertical | 0.5 | Range/stability | | | | TRUE | Table | 274 | 24.38497802 | 0.097087776 | -0.01342857 | 0.094965761 | 72.17648718 | 0.028651314 |
| SAW Data 2011-09-28 12.25.26.txt | NS401R | 4: Rotated Horizontal | 0.5 | Range/stability | | | | TRUE | Table | 312 | 23.81866881 | 0.309237318 | -0.029241158 | 0.300428838 | 58.75350804 | 0.12139947 |
| SAW Data 2011-09-28 12.47.28.txt | NS401R | 1: Vertical | 0.75 | Range/stability | | | | TRUE | Table | 285 | 24.08515493 | 0.096493453 | -0.006735915 | 0.091936512 | 68.47215141 | 0.048237578 |
| SAW Data 2011-09-28 13.15.21.txt | NS401R | 2: Horizontal | 0.75 | Range/stability | | | | TRUE | Table | 495 | -9.266022267 | 57.89860595 | 6.036251012 | 57.6592758 | 32.14439879 | 1.45650392 |
| SAW Data 2011-09-28 13.50.41.txt | NS401R | 3: Rotated Vertical | 0.75 | Range/stability | | | | TRUE | Table | 268 | 24.12127715 | 0.096819526 | -0.001962547 | 0.083298666 | 69.09417603 | 0.051178898 |
| SAW Data 2011-09-28 14.07.16.txt | NS401R | 4: Rotated Horizontal | 0.75 | Range/stability | | | | TRUE | Table | 357 | 23.61545787 | 0.658856206 | -0.12602809 | 0.645692745 | 53.78781742 | 0.209205035 |
| SAW Data 2011-09-28 14.30.11.txt | NS401R | 5: Flat Inline | 0.75 | Range/stability | | | | TRUE | Table | 273 | 18.83683824 | 18.98455798 | -3.900830882 | 18.87323206 | 37.89798529 | 1.290807862 |
| SAW Data 2011-09-28 14.46.54.txt | NS401R | 6: Flat Perpendicular | 0.75 | Range/stability | | | | TRUE | Table | 451 | -8.308531111 | 53.7371796 | 2.473884444 | 54.44036563 | 32.87587111 | 1.415200853 |
| SAW Data 2011-09-28 15.16.20.txt | NS401R | 1: Vertical | 1 | Range/stability | | | | TRUE | Table | 292 | 23.51962199 | 0.2402966 | -0.043611684 | 0.239416079 | 64.36876976 | 0.616364786 |
| SAW Data 2011-09-28 15.34.22.txt | NS401R | 2: Horizontal | 1 | Range/stability | | | | TRUE | Table | 393 | -1.448857143 | 58.59791447 | 1.206219388 | 56.89453872 | 32.59671173 | 1.425130534 |
| SAW Data 2011-09-28 16.04.52.txt | NS401R | 3: Rotated Vertical | 1 | Range/stability | | | | TRUE | Table | 332 | 23.54883082 | 0.192906649 | -0.0398429 | 0.192172822 | 64.68635952 | 0.064422804 |
| SAW Data 2011-09-28 16.25.41.txt | NS401R | 4: Rotated Horizontal | 1 | Range/stability | | | | TRUE | Table | 308 | 23.69815635 | 1.257851907 | -0.127710098 | 1.217939983 | 48.10444951 | 0.410088497 |
| SAW Data 2011-09-28 16.44.57.txt | NS401R | 5: Flat Inline | 1 | Range/stability | | | | TRUE | Table | 316 | 10.36121905 | 47.44967905 | -8.365838095 | 47.26379408 | 33.66790794 | 1.410691979 |
| SAW Data 2011-09-28 17.04.26.txt | NS401R | 6: Flat Perpendicular | 1 | Range/stability | | | | TRUE | Table | 520 | -4.591714836 | 58.72776358 | 6.189171494 | 58.69877105 | 32.02245087 | 1.395904706 |
| SAW Data 2011-09-29 09.53.22.txt | NS401R | 5: Flat Inline | 0.25 | Range/stability | | | | TRUE | Table | 341 | 23.93764706 | 1.160596637 | -0.065258824 | 1.136860404 | 49.21919706 | 0.354298267 |
| SAW Data 2011-09-29 10.13.32.txt | NS401R | 6: Flat Perpendicular | 0.25 | Range/stability | | | | TRUE | Table | 320 | 23.83270219 | 3.832336271 | -0.33584326 | 3.781371431 | 40.56337931 | 1.0289986 |
| SAW Data 2011-09-29 10.34.05.txt | NS401R | 5: Flat Inline | 0.5 | Range/stability | | | | TRUE | Table | 318 | 23.9937079 | 2.041987371 | -0.146277603 | 2.016572356 | 44.18775079 | 0.662552872 |
| SAW Data 2011-09-29 10.53.30.txt | NS401R | 6: Flat Perpendicular | 0.5 | Range/stability | | | | TRUE | Table | 762 | 16.31105913 | 33.3049348 | -5.291929041 | 33.09736187 | 35.67306833 | 1.410643559 |
| SAW Data 2011-09-29 11.38.38.txt | NS401R | 1: Vertical | 0.25 | Range/stability | Repeat with correlation peak functionality. | | | TRUE | Table | 311 | 24.52891548 | 0.288060127 | -0.019470968 | 0.229243114 | 73.79729677 | 0.057037154 |
| SAW Data 2011-09-29 11.57.33.txt | NS401R | 1: Vertical | 0.25 | Range/stability | Repeat with correlation peak functionality. | | | TRUE | Table | 289 | 17.78694097 | 28.7351483 | -5.377625 | 28.59469561 | 37.13689583 | 1.364251894 |
| SAW Data 2011-09-29 12.15.00.txt | NS401R | 3: Rotated Vertical | 0.25 | Range/stability | Repeat with correlation peak functionality. | | | TRUE | Table | 293 | 24.74587329 | 0.378576972 | -0.032184932 | 0.266065726 | 73.88864726 | 0.057100763 |
| SAW Data 2011-09-29 12.32.56.txt | NS401R | 4: Rotated Horizontal | 0.25 | Range/stability | | | | TRUE | Table | 285 | 23.87126761 | 0.153680841 | -0.018616197 | 0.150344706 | 65.10253873 | 0.063433295 |
| SAW Data 2011-09-29 15.49.00.txt | NS402 | 1: Vertical | 0.25 | Range/stability | | | | TRUE | Table | 285 | 28.74114437 | 1.098886113 | 0.244320423 | 1.256900565 | 74.26085563 | 0.035510037 |
| SAW Data 2011-09-30 10.19.43.txt | NS402 | 2: Horizontal | 0.25 | Range/stability | | | | TRUE | Table | 298 | 22.11603367 | 0.894780903 | -0.041407407 | 0.880512508 | 54.69873064 | 0.2389257 |
| SAW Data 2011-09-30 10.40.54.txt | NS402 | 3: Rotated Vertical | 0.25 | Range/stability | | | | TRUE | Table | 299 | 28.67918792 | 0.942761849 | 0.075436242 | 1.185823985 | 74.25665772 | 0.02720932 |
| SAW Data 2011-09-30 11.02.11.txt | NS402 | 4: Rotated Horizontal | 0.25 | Range/stability | | | | TRUE | Table | 298 | 25.19660943 | 0.173984959 | 0.003905724 | 0.169517512 | 69.57240404 | 0.060151709 |
| SAW Data 2011-09-30 11.44.12.txt | NS402 | 5: Flat Inline | 0.25 | Range/stability | | | | TRUE | Table | 273 | 25.277625 | 0.670243547 | 0.028869706 | 0.649941702 | 53.31743382 | 0.172150848 |
| SAW Data 2011-09-30 12.27.15.txt | NS402 | 6: Flat Perpendicular | 0.25 | Range/stability | | | | TRUE | Table | 298 | 26.13785859 | 1.681480789 | 0.23730303 | 1.653615985 | 49.45698316 | 0.252425537 |
| SAW Data 2011-09-30 14.32.25.txt | NS402 | 1: Vertical | 0.5 | Range/stability | | | | TRUE | Table | 330 | 24.96277204 | 0.104064208 | 0.009696605 | 0.103997528 | 72.83291489 | 0.042634994 |
| SAW Data 2011-09-30 14.50.31.txt | NS402 | 2: Horizontal | 0.5 | Range/stability | | | | TRUE | Table | 350 | 24.81387966 | 0.649466892 | -0.015610315 | 0.391230233 | 59.2582894 | 0.213323279 |
| SAW Data 2011-09-30 15.12.55.txt | NS402 | 3: Rotated Vertical | 0.5 | Range/stability | | | | TRUE | Table | 361 | 26.73690278 | 0.48501212 | -0.200211111 | 0.480795493 | 72.97194167 | 0.042757129 |
| SAW Data 2011-09-30 15.31.12.txt | NS402 | 4: Rotated Horizontal | 0.5 | Range/stability | | | | TRUE | Table | 717 | 23.22272626 | 0.944936356 | 0.024121508 | 0.941690152 | 53.05921369 | 0.166560585 |
| SAW Data 2011-09-30 15.53.15.txt | NS402 | 5: Flat Inline | 0.5 | Range/stability | | | | TRUE | Table | 745 | 26.27657393 | 0.753605051 | 0.014032258 | 0.664232008 | 54.3018871 | 0.235226447 |
| SAW Data 2011-09-30 16.38.41.txt | NS402 | 6: Flat Perpendicular | 0.5 | Range/stability | | | | TRUE | Table | 2157 | 18.38978154 | 3.860121412 | 0.279324675 | 4.038837967 | 47.15324536 | 0.315299157 |
| SAW Data 2011-09-30 17.00.45.txt | NS402 | 1: Vertical | 0.75 | Range/stability | | | | TRUE | Table | 284 | 29.6289540 | 0.253003941 | 0.041187279 | 0.235300042 | 73.29104594 | 0.030187852 |
| SAW Data 2011-10-03 09.55.02.txt | NS402 | 2: Horizontal | 0.75 | Range/stability | | | | TRUE | Table | 373 | 25.19426075 | 0.158429776 | 0.00775 | 0.149341247 | 67.09383871 | 0.045837587 |
| SAW Data 2011-10-03 10.14.12.txt | NS402 | 3: Rotated Vertical | 0.75 | Range/stability | | | | TRUE | Table | 285 | 28.63623944 | 0.641382054 | 0.018887324 | 0.676546156 | 73.60568662 | 0.012075017 |
| SAW Data 2011-10-03 10.42.05.txt | NS402 | 4: Rotated Horizontal | 0.75 | Range/stability | | | | TRUE | Table | 363 | 22.45159558 | 0.360812116 | 0.033964088 | 0.342979694 | 63.54331768 | 0.119385018 |
| SAW Data 2011-10-03 11.05.27.txt | NS402 | 5: Flat Inline | 0.75 | Range/stability | | | | TRUE | Table | 760 | 20.29211331 | 0.292279672 | 0.028710145 | 0.288670431 | 54.72339657 | 0.130915478 |
| SAW Data 2011-10-03 11.22.55.txt | NS402 | 6: Flat Perpendicular | 0.75 | Range/stability | | | | TRUE | Table | 358 | 22.67236134 | 1.184008242 | 0.071963585 | 1.19701294 | 51.55857703 | 0.187954701 |
| SAW Data 2011-10-03 12.02.50.txt | NS402 | 7: Horizontal Flipped | 0.75 | Range/stability | | | | TRUE | Table | 358 | 24.76250981 | 1.8713201 | -0.115100084 | 1.80441701 | 47.08087395 | 0.31192887 |
| SAW Data 2011-10-05 10.40.09.txt | NS402 | 1: Vertical | 1 | Range/stability | | | | TRUE | Table | 336 | 27.5526209 | 0.280954696 | -0.02666059 | 0.278756499 | 73.70961194 | 0.029770356 |
| SAW Data 2011-10-05 11.00.23.txt | NS402 | 2: Horizontal | 1 | Range/stability | | | | TRUE | Table | 338 | 20.18833234 | 0.758498954 | -0.009433234 | 0.737457825 | 51.3402997 | 0.250881272 |
| SAW Data 2011-10-05 14.05.47.txt | NS402 | 3: Rotated Vertical | 1 | Range/stability | | | | TRUE | Table | 389 | 24.44219742 | 0.332925281 | -0.042507732 | 0.313887844 | 71.20562113 | 0.049666779 |
| SAW Data 2011-10-05 15.37.05.txt | NS402 | 4: Rotated Horizontal | 1 | Range/stability | | | | TRUE | Table | 277 | 20.75972826 | 0.351222419 | 0.056690579 | 0.335175642 | 63.36808696 | 0.077932883 |
| SAW Data 2011-10-05 11.22.55.txt | NS402 | 5: Flat Inline | 1 | Range/stability | | | | TRUE | Table | 650 | 25.00006934 | 0.600707538 | -0.065958398 | 0.597203663 | 52.96111402 | 0.175067631 |
| SAW Data 2011-10-05 12.02.50.txt | NS402 | 6: Flat Perpendicular | 1 | Range/stability | | | | TRUE | Table | 406 | 22.7696 | 3.355107656 | -0.147266667 | 3.296120856 | 40.70310012 | 0.666709918 |
| SAW Data 2011-10-05 10.40.09.txt | NS403R | 1: Vertical | 1 | Range/stability | | 22.7 | 22.9 | TRUE | Table | 322 | 17.14851402 | 0.254153953 | 0.251507592 | 0.248507795 | 70.87387539 | 0.058611566 |
| SAW Data 2011-10-05 11.00.23.txt | NS403R | 2: Horizontal | 1 | Range/stability | | 22.9 | 22.8 | TRUE | Table | 923 | 18.6289577 | 3.165683707 | 0.251507592 | 3.164919317 | 47.39646855 | 0.467508887 |
| SAW Data 2011-10-05 14.05.47.txt | NS403R | 3: Rotated Vertical | 1 | Range/stability | | 22.6 | 22.9 | TRUE | Table | 1585 | 18.25395833 | 0.248622293 | -0.009633576 | 0.237769306 | 69.90869886 | 0.047428101 |
| SAW Data 2011-10-05 15.37.05.txt | NS403R | 4: Rotated Horizontal | 1 | Range/stability | | 23 | 23 | TRUE | Table | 430 | 18.63766434 | 1.259993324 | 0.107876457 | 1.337779502 | 54.57328904 | 0.165592009 |

| File | Sensor | Orientation | Distance (m) | Test | Notes | Temperature (°C) Start | Temperature (°C) Stop | Exhaust Fans | Location | Rows | Temperature Average (°C) | Temperature Std Dev (°C) | Residual (21-point median) Average (°C) | Residual (21-point median) Std Dev (°C) | Correlation Peak Average (dB) | Correlation Peak Std Dev (dB) |
|---|---|---|---|---|---|---|---|---|---|---|---|---|---|---|---|---|
| SAW Data 2011-10-05 16.03.22.txt | NS403R | 5: Flat Inline | 1 | Range/stability | | 23.1 | 23.3 | TRUE | Table | 274 | 28.2525148 | 11.48862814 | 1.485164835 | 11.41506661 | 42.56429513 | 0.666061775 |
| SAW Data 2011-10-05 16.20.53.txt | NS403R | 6: Flat Perpendicular | 1 | Range/stability | | 23.3 | 23.4 | TRUE | Table | 1950 | -2.38819548 | 58.11558643 | 0.328156491 | 57.8079421 | 33.15069318 | 1.384540142 |
| SAW Data 2011-10-06 15.12.51.txt | NS401R | 1: Vertical | 6.55 | Range/stability | Corner to corner. | 23.4 | 23.5 | TRUE | Tripods | 366 | 14.28738356 | 57.73208957 | -0.741493151 | 57.3149256 | 32.78839452 | 1.123726387 |
| SAW Data 2011-10-06 16.39.17.txt | NS401R | 1: Vertical | 6 | Range/stability | | 23.6 | 23.4 | TRUE | Tripods | 967 | 13.15324638 | 42.77217493 | -1.42855383 | 42.27491829 | 34.46324327 | 1.21933671 |
| SAW Data 2011-10-06 17.51.40.txt | NS401R | 1: Vertical | 5 | Range/stability | | 23.4 | 23.3 | TRUE | Tripods | 387 | -8.413533679 | 61.94454637 | 8.581779793 | 61.55122722 | 32.84259585 | 1.166587539 |
| SAW Data 2011-10-07 10.17.12.txt | NS401R | 1: Vertical | 4 | Range/stability | | 23.2 | 23.1 | TRUE | Tripods | 739 | 21.04142683 | 10.29289891 | -0.422271003 | 10.30094208 | 38.64418699 | 1.069440727 |
| SAW Data 2011-10-07 11.03.03.txt | NS401R | 1: Vertical | 3 | Range/stability | | 23.1 | 23.3 | TRUE | Tripods | 884 | 25.28935787 | 6.204173513 | -0.376938845 | 6.196697754 | 40.77924915 | 0.814676798 |
| SAW Data 2011-10-07 11.56.55.txt | NS401R | 1: Vertical | 2.5 | Range/stability | | 23.2 | 23.1 | TRUE | Tripods | 463 | 25.44919697 | 2.66028152 | -0.096279221 | 2.60674229 | 43.18748701 | 0.61294368 |
| SAW Data 2011-10-07 12.28.45.txt | NS401R | 1: Vertical | 2 | Range/stability | | 23.3 | 23.1 | TRUE | Tripods | 1187 | 24.55265599 | 1.679446434 | -0.062162732 | 1.653363888 | 45.76545025 | 0.459377213 |
| SAW Data 2011-10-07 13.39.43.txt | NS401R | 1: Vertical | 1.5 | Range/stability | | 23.2 | 23.4 | TRUE | Tripods | 517 | 22.9341938 | 1.106488158 | -0.305151163 | 1.108600113 | 53.08113372 | 0.200540482 |
| SAW Data 2011-10-07 14.13.56.txt | NS401R | 1: Vertical | 1 | Range/stability | | 23.4 | 23.4 | TRUE | Tripods | 644 | 23.5421846 | 0.496522968 | -0.085279938 | 0.486223141 | 56.39411571 | 0.148488946 |
| SAW Data 2011-10-07 15.02.38.txt | NS401R | 1: Vertical | 0.5 | Range/stability | | 23.4 | 23.3 | TRUE | Tripods | 1849 | 23.93889069 | 0.117137432 | -0.013498918 | 0.111302935 | 68.52789989 | 0.052674885 |
| SAW Data 2011-10-07 16.49.32.txt | NS401R | 1: Vertical | 1 | Range/stability | Repeat to ensure no baseline shift. | 23.4 | 23.3 | TRUE | Table | 577 | 23.44966146 | 0.534921018 | -0.125592014 | 0.527820485 | 56.49888021 | 0.1668771 |
| SAW Data 2011-10-12 13.08.14.txt | NS404 | 1: Vertical | 1 | Range/stability | | 22.5 | 22.4 | TRUE | Table | 413 | 30.2971966 | 0.684573757 | 0.18482767 | 0.68080214 | 64.81487379 | 0.059482223 |
| SAW Data 2011-10-12 13.41.39.txt | NS404 | 2: Horizontal | 1 | Range/stability | | 22.4 | 22.4 | TRUE | Table | 281 | 31.98131071 | 69.32769036 | -0.325585714 | 71.32300126 | 30.91911071 | 1.44257943 |
| SAW Data 2011-10-12 13.59.37.txt | NS404 | 3: Rotated Vertical | 1 | Range/stability | | 22.4 | 22.5 | TRUE | Table | 321 | 32.359625 | 0.222332287 | -0.018771875 | 0.219544487 | 61.45579375 | 0.086043919 |
| SAW Data 2011-10-12 14.19.45.txt | NS404 | 4: Rotated Horizontal | 1 | Range/stability | | 22.5 | 22.4 | TRUE | Table | 514 | 27.50284795 | 1.759779925 | 0.118758285 | 1.768820764 | 46.42036842 | 0.389633811 |
| SAW Data 2011-10-12 14.50.46.txt | NS404 | 5: Flat Inline | 1 | Range/stability | | 22.4 | 22.3 | TRUE | Table | 450 | 28.13257906 | 21.21006529 | -0.497131403 | 21.10532334 | 35.44454788 | 1.26339868 |
| SAW Data 2011-10-12 15.18.16.txt | NS404 | 6: Flat Perpendicular | 1 | Range/stability | | 22.3 | 22.4 | TRUE | Table | 602 | 45.61572712 | 74.53222599 | -18.58746589 | 76.87694771 | 29.98282696 | 1.482466014 |
| SAW Data 2011-10-12 15.55.21.txt | NS404 | 7: Horizontal Flipped | 1 | Range/stability | | 22.4 | 22.4 | TRUE | Table | 716 | 27.75298042 | 1.166072321 | -0.11009035 | 1.148234786 | 50.25758601 | 0.259367831 |
| SAW Data 2011-10-12 16.38.23.txt | NS404 | 7: Horizontal Flipped | 0.75 | Range/stability | | 22.3 | 21.9 | TRUE | Table | 600 | 25.76162938 | 3.273086831 | -0.033903172 | 3.256498183 | 41.01158097 | 0.753355045 |
| SAW Data 2011-10-12 17.14.16.txt | NS404 | 7: Horizontal Flipped | 0.5 | Range/stability | | 21.9 | 21.6 | TRUE | Table | 315 | 22.99021656 | 2.150856691 | -0.095557325 | 2.139236739 | 44.32104459 | 0.485641308 |
| SAW Data 2011-10-12 17.33.40.txt | NS404 | 7: Horizontal Flipped | 0.25 | Range/stability | | 21.8 | 21.5 | TRUE | Table | 598 | 26.24640034 | 0.281399932 | 0.029142379 | 0.278447406 | 60.2019732 | 0.088655596 |